LARAMIDE STRESS CONDITIONS AND DEFORMATION MECHANISMS DURING THE FORMATION OF HUDSON AND DALLAS DOMES, LANDER QUADRANGLE, WIND RIVER MOUNTAINS, LANDER, WYOMING

A Thesis presented to the Faculty of the Graduate School
University of Missouri

In Partial Fulfillment
Of the Requirements for the Degree

Master of Science

---

by

JAMES WESLEY CLEMENTS

Dr. Robert L. Bauer, Thesis Supervisor

MAY 2008

The undersigned, appointed by the Dean of the Graduate School, have examined the thesis entitled

LARAMIDE STRESS CONDITIONS AND DEFORMATION MECHANISMS DURING THE FORMATION OF DALLAS AND HUDSON DOMES, LANDER QUADRANGLE, WIND RIVER MOUNTAINS, LANDER, WYOMING

Presented by James Wesley Clements

A candidate for the degree of Master of Science

And hereby certify that in their opinion it is worthy of acceptance.

Professor Robert Bauer

Professor Francisco Gomez

Professor Erik Loehr

ACKNOWLEDGEMENTS

First, I would like to thank those who funded this research. The USGS Educational Mapping Program (EDMap), in cooperation with the Wyoming Geological Survey (WSGS), supported by field work and map publication. The Geological Society of America (GSA) helped fund research pertaining to structural problems associated with the Laramide structure formation.

Thanks to the University of Missouri and the department of Geological Sciences for the educational background and teaching assistantship that allowed me to prepare for my research.

Thanks to the University of Missouri Branson Field Laboratory for hosting me during one summer of educational experience and during my summer of research. The camp facilities provided me with a wonderful place to conduct and complete my research, with excellent sources of knowledge of the study area from visiting professors and literature collected over the several decades the camp has been in operation.

I would also like to thank the hundreds of private landowners who graciously allowed me to cruise around on their property, as well as Citation Oil and Gas for permission to map on their land.

TABLE OF CONTENTS

LIST OF FIGURES

Figure Page

LIST OF TABLES

Table Page

LIST OF PLATES

ABSTRACT

Laramide fold forms along the northeastern flank of the Wind River Mountains in west central Wyoming include a series of doubly plunging folds arranged in a left-stepping en echelon pattern. The fold patterns and geometries are derived from regional scale tectonic stresses that have been complicated by local stress conditions associated with buckle folding and potential basement involved faulting (forced folding). The purpose of this study was to determine the fold-inducing mechanisms forming Dallas Dome, a doubly plunging asymmetric anticline verging toward the core of the Wind River Mountains. The study involved geologic mapping of surface deformation, collecting and analyzing fault and fracture orientation data, and interpreting the results to deduce the fold's deformation geometry, the folding mechanisms and associated stresses. Mapping and well log constraints indicate that the geometry of the fold form is a result of local basement involved faulting, propagating upward into a dual thrust system in the overlying sedimentary units. The offset on the dual thrust system diminishes northward, where forelimb strata become decreasingly tilted and basement offset diminishes.

Regional fracture sets R1 (45/225) and R2 (75/255) were determined to be directly associated with maximum principal shortening directions during Laramide and Sevier Orogenies, respectively. Fold induced fracture sets include J1 (60/240), J2 (160/340), J3 (105/285), and J4 (55/235; 65/245). J1 was determined to be an extensional fracture set oriented sub-perpendicular to the

fold hinge of Dallas Dome, and is thus associated with the buckle folding mechanism. J2 strikes sub-parallel to the fold hinge of Dallas Dome with variable dip angles consistent with a conjugate shear set bisected by an associated extensional fracture set. As such, J2 could be associated with either buckle or forced folding. J3 is a conjugate shear set whose dip values range from 60-90-60 and is indicative of vertical stresses associated with forced folding. However, the orientation of J3 with respect to the hingeline of Dallas Dome is not consistent with either forced folding or buckle folding models. The origin of this fracture set is unclear. Finally, J4 is a conjugate fracture set that is subparallel to normal faults that occur in the southern part of the study area, near the interchange with Derby Dome, and are interpreted as a response to extension associated with the en echelon interchange between Derby and Dallas Domes.

CHAPTER I: INTRODUCTION

The origin of basement-involved, Laramide, uplifts in the foreland of the western cordillera of North America (the Rocky Mountains) has been debated for many years (Berg, 1961; Blackstone, 1993; Brown, 1987; Erslev, 1993; Hamilton, 1981). Deformation typically terminates in a mountain foreland as fold-and-thrust belts that are restricted to the sedimentary cover. However, Laramide tectonism in the Rocky Mountains produced a series Precambrian cored uplifts along reverse faults, all of which lie east (in the foreland) of the Sevier fold-and-thrust belt (Fig. 1). This distinct style of deformation has invoked three levels of discussion. First, what was the tectonic nature of the western margin of North America that produced the Laramide uplifts (Bird, 1983; DeCelles, 2004; Dickinson and Snyder, 1978)? Second, was the force that produced the Laramide uplifts primarily vertical, or primarily horizontal (Berg, 1961; Stearns, 1971)? Third, how did this regional stress regime produce the various uplifts and their associated features (Brown, 1988; Gries, 1982)? The question of vertical versus horizontal tectonic stresses has been the focus of many studies (and contentious debate) across the Rock Mountains, but some of the most significant studies examined the Wind River Mountains of west-central Wyoming. Berg (1961) first postulated that the Precambrian cored Wind River Mountains were uplifted along a thrust fault that overlies an overturned sedimentary sequence along the southwestern margin of the mountain range. This hypothesis was later confirmed by the Consortium for Continental Reflection Profiling (COCORP) in a study that involved a deep seismic reflection profile across the range and into the Wind River basin (Brewer, Smithson et al, 1980). The study found that the range was uplifted along a shallow reverse fault, dipping to the northeast at approximately thirty degrees (Brewer, Smithson et al, 1980). As such, results of this study strongly favors the horizontal compression hypothesis.

DeCelles, P.G., 2004, Late Jurassic to Eocene evolution of the Cordilleran thrust belt and foreland basin system, western U.S.A.: American Journal of Science, v. 304, no. 2, p. 105.

Figure 1: Tectonic map of the Western Cordillera of North America. Light gray indicates extent of Sevier Orogeny, while bladed area indicates extent of Laramide deformation (Decelles, 2004).

Most researchers now accept that horizontal forces produced the Laramide uplifts. Many studies in the Rocky Mountains are now focused on determining the regional stress orientations that produced the Laramide deformation features and the tectonic regimes that produced the stress responsible for these features. Bird (1998) first compiled all available kinematic data from the foreland region in order to create a kinematic model that would depict regional stress evolution during the Laramide orogeny. He concluded that Laramide stresses were oriented E-W during earlier Laramide time, but later shifted to a NE-SW orientation. This shift in orientation has been associated with plate interactions along the margin of western North America, when the Farallon Plate began subducting beneath the North American Plate at a relatively shallow angle (Fig. 2).

Bunge, H. P., and Grand, S. P., 2000,
Mesozoic plate-motion history below the
northeast Pacific Ocean from seismic
images of the subducted Farallon Slab:
Nature, v. 405, no. 6784, p. 337-340.

Figure 2: Plate tectonic map showing relationship between Kula, Farallon, and North American Plates during Laramide time (Bunge and Grande, 2000).

Laramide regional stress states are expressed throughout much of the Rocky Mountain foreland. Major uplifts throughout the region strike perpendicular to Bird's Laramide regional stress orientation of NE-SW. This is particularly true of the Wind River Mountains, located in west central Wyoming. The Wind River Mountains were uplifted along a shallow reverse fault that is exposed along the southwestern margin of the uplift. Uplift exposed the Precambrian core of the range and tilted the sedimentary cover to the northeast.

Several studies along the northeastern flank of the Wind River Mountains have investigated a series smaller scale periclinal folds, including Hudson, Dallas, and Derby Domes (Fig. 3), that mimic the overall orientation of the range (Willis and Groshong, 1993; Craddock and Relle, 2003; Abercrombie, 1988; Kightlinger, 1997). These studies have been important in testing hypotheses developed for regional stress regimes that produced Laramide uplifts, but have been complicated by local stresses developing as a result of uplift of the Wind River Mountains and tilting of the sedimentary cover.

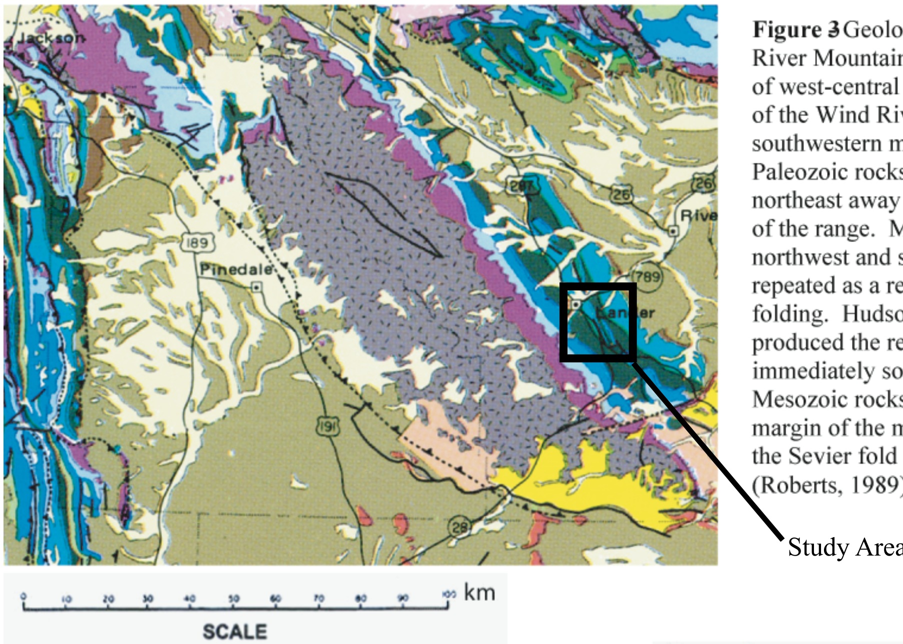

Figure 3 Geologic map of the Wind River Mountains and adjacent areas of west-central Wyoming. The trace of the Wind River thrust is along the southwestern margin of the range. Paleozoic rocks dip uniformly to the northeast away from the uplifted core of the range. Mesozoic rocks to the northwest and southeast of Lander are repeated as a result of basin-margin folding. Hudson and Dallas domes produced the repeated Mesozoic section immediately southeast of Lander. Mesozoic rocks along the western margin of the map are deformed by the Sevier fold and thrust belt. (from (Roberts, 1989)

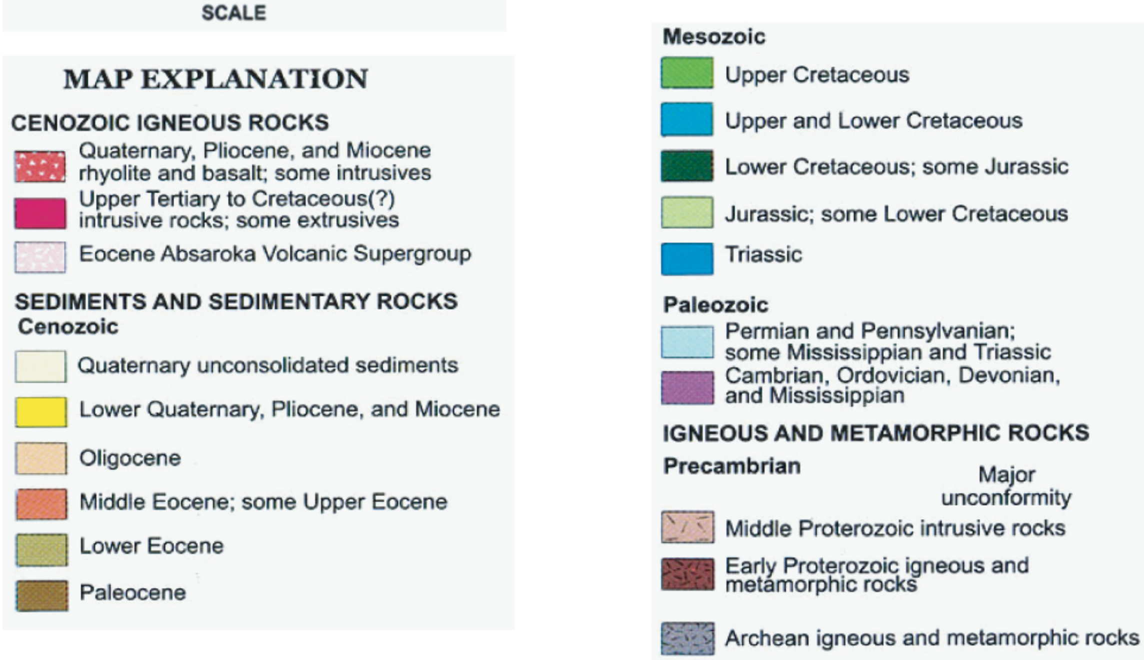

Hudson, Dallas, and Derby Domes formed along the basin margin of the Wind River Mountains (Fig. 3) and mimic the overall orientation of the Wind River Mountains, but they are offset in a left-stepping en echelon pattern toward the north. These features have been the topic of debate which stems from their association with regional and local stress regimes (Willis and Groshong, 1993; Craddock and Relle, 2003; Brocka, 2007; Kightlinger, 1997). That is, are such features associated with local stresses that stem from tilting of the sedimentary cover, which results in space constrictions along the basin, or are they a result of smaller scale basement involved faulting? The COCORP seismic profile provides support for both end member hypothesis, but does not provide conclusive evidence for all small scale features. Further studies by Brocka (2007) determined that southern portions of Dallas Dome, Derby Dome, and northern portions of Sheep Mountain Anticline were the result of both local and regional stresses. However, further investigation is needed in order to test these conclusions.

The purpose of this study is to evaluate the mechanism of formation of Dallas and Hudson Domes using a combination of geological and structural mapping and fractures analysis. There are three principal components to this evaluation: 1) to determine whether forced folding, associated with local basement faulting, affected the domes, 2) to determine to what degree buckle folding, associated with regional stresses, produced the domes and their features, and 3) evaluate the degree to which local and regional stresses contributed to the folding process and to the interchange between Dallas and Hudson Domes. Brocka (2007) hypothesized that deformation and formation of the domes were a result of local basement faulting associated with regional stresses. I will test this hypothesis by comparing his results with my analysis to determine if any alternative hypotheses are plausible.

The specific objectives of this study, in order, were to:

1. Map the distribution of rock formations and deformation features contained within the Lander 7.5' Quadrangle and adjacent areas, which contain the majority of Dallas Dome and the adjacent interchange with Hudson Dome to the north.
2. Collect representative fault and fracture orientation data within the area.
3. Determine how the fault and fracture data are related to the mechanics of formation of Dallas and Hudson Domes. Are there fractures and faults associated with forced folding, buckle folding or some combination of these two mechanisms?
4. Determine whether the data and interpretations from Hudson and Dallas Domes are consistent observations and interpretations of Brocka (2007) for Derby Dome and its interchange with Dallas Dome and Sheep Mountain.
5. Evaluate whether the regional stress regimes inferred to have affected Hudson and Dallas Domes are consistent with those inferred for other similar Laramide structures associated with the broad region of the Laramide orogen.

<u>Location</u>

The study area is located on the northeastern flank of the Wind River Mountains in west-central Wyoming. Dallas Dome is one of several doubly plunging anticlines that flank the Wind River Mountains, with Hudson Dome to its north and Derby Dome and Sheep Mountain anticline to its south (Fig. 4). These features are left laterally offset and trend in a general northwest-southeast orientation. Dallas Dome is located along highway 287, five to ten miles from Lander, Wyoming (Fig. 4). The study area is contained almost entirely within the Lander 7.5" Quadrangle, but is also contained within the Wolf Point, Lander SE, and Weiser Pass 7.5" Quadrangles.

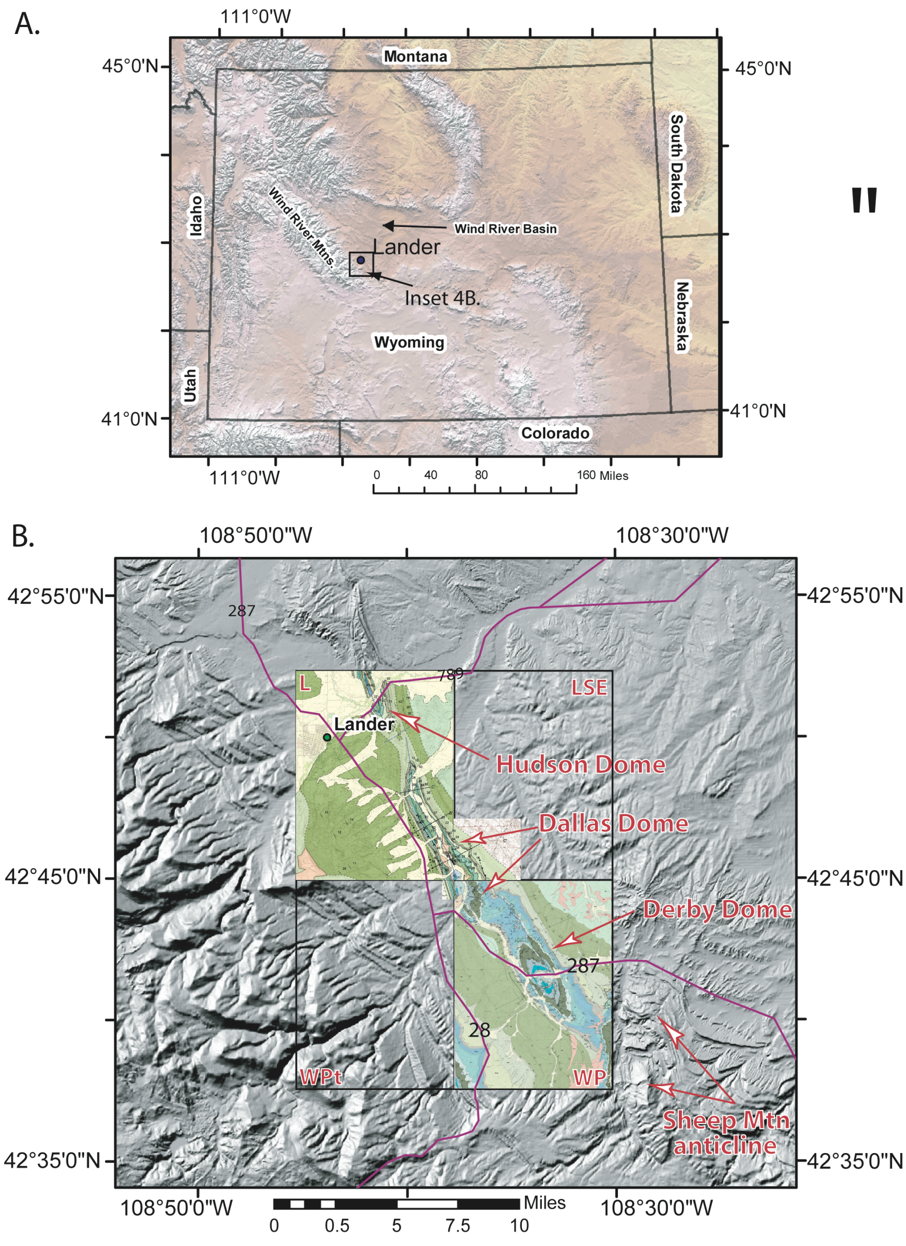

Figure 4: Physiographic map of the study area. Individual gray boxes in 4B indicate the Lander (L), Lander SE (LSE), Wolf Point (WPt), and Weiser Pass (WP) 7.5' Quadrangles.

Geologic Setting

The study area lies near the western edge of Laramide deformation in the Rocky Mountain foreland of North America (Fig. 1). Laramide uplifts are distributed along the eastern extent of the North American Cordillera in the western United States, just east of the fold-and-thrust belt formed during the Sevier Orogeny (140-65Ma). The Laramide Rocky Mountains are especially distinct, because there are no other instances where basement involved uplifts occur 1200km-1800km from the zone of plate convergence (Fig. 2).

The stresses that produced these uplifts have been associated with the subduction of relatively hot, buoyant lithosphere of the Kula and Farallon Plates beneath the North American Plate. Work by Coney (1978) suggests that the convergence rate between the two active plates was about 14 cm/yr in a northeast-southwest direction (Fig. 2). As a result, much of the stress was horizontally oriented and concentrated within the North American lithosphere. This process is a widely accepted mechanism for stress fields that induced Laramide uplifts and the associated flank structures, but because of the variable orientations of Laramide uplifts, their origins and relationships to principal stress regimes remains unclear (Willis and Groshong, 1993; Bunge and Grande, 2000; Dickenson and others, 1988).

The Wind River Mountains are some of the largest and best studied Laramide uplifts. The range is oriented northwest-southeast, normal to the regional maximum principal stress produced by the shallow subduction of the Farallon Plate. The Wind River Mountains were the focus of studies by Berg (1962), who concluded that the uplift was a response a fold-thrust mechanism that uplifted Precambrian basement over the sedimentary cover along a relatively shallow thrust fault along the southwestern margin of the uplift. A subsequent COCORP seismic reflection profile later (Brewer, Smithson et al, 1980) later identified the orientation of the Wind River Thrust (Fig. 5). These results indicated the thrust had a dip of about thirty degrees and that Precambrian basement had been horizontally displaced a minimum of 21km and offset vertically almost 14km along the thrust. Furthermore, the offset resulted in a tilting of the sedimentary cover by ten to fifteen degrees eastward. The dip slope continues to the northeast toward the basin until it is interrupted by flank fold features such as Hudson, Dallas, and Derby Domes considered in this study.

Brewer, J. A., Smithson, S. B., Oliver, J. E., Kaufman, S., and Brown, L. D., 1980, The Laramide Orogeny; evidence from COCORP deep crustal seismic profiles in the Wind River Mountains, Wyoming: Tectonophysics, v. 62, no. 3-4, p. 165.

Figure 5: COCORP seismic reflection profile across the Wind River Mountains and into the Wind River Basin. Profile clearly depicts the Wind River Thrust, as well as displacement on subsidiary reverse faults near the basin (Brewer, Smithson et al, 1980).

These fold structures form against the base of the Wind River dip slope (WRDS), and are expressed as asymmetrical doubly plunging periclinal folds (locally referred to as domes) that are offset laterally from one another in a left stepping en echelon pattern. The dome structures expose a series of Mesozoic rock units underlain by Paleozoic rock units (Abercrombie, 1988; Kightlighter; 1997 Willis and Groshong, 1993). Features within the study area include Dallas Dome, a strongly asymmetrical, west verging pericline, and the southern part of Hudson Dome, a slightly asymmetrical east verging pericline. Both structures serve as important culminations for the concentration of oil. In the following text, I refer to the Hudson Dome and Dallas Dome fold line as the HDFL.

Fold structures along the Wind River Basin margin, like Dallas and Hudson Dome, have been the focus of many studies to determine: (1) the relationship of regionally stresses to the formation of the structures (Berg, 1961; Brown, 1988; 1993; Willis and Groshong, 1993), (2) what mechanisms are induced by local stresses (Willis and Groshong, 1993), (3) the relationship of local stresses to the formation of the deformation features (Kightlinger, 1997; Abercrombie, 1989), (4) the deformational history of the HDFL(Willis and Groshong, 1997; Craddock and Relle, 2003), and (5) the relationship of the deformation to structural oil traps? Based on a regional mapping study of the Wind River Basin, Keefer (1970) concluded that the basin margin flank structures were associated with the shape of the larger uplifts. Willis and Groshong (1993) later completed a more specific study along the entire line of folded flank structures, describing each fold structure and their geometries. Their study focused on mechanisms that produced the local folding and faulting, and their en-echelon displacements. Their study confirmed the presence of secondary “crowd” structures such as those described by Brown (1988, 1993) (Fig. 6). Crowd structures like these occur as a result of space problems created during layer-parallel slip and gradual tightening of folded sedimentary rock. Examples of various crowd structures occur across the study are and adjacent regions. Masters theses by Abercrombie (1989) and Kightlinger (1997), and a senior thesis by Meinen (1993) completed detailed structural mapping and analysis of individual folds to provide an understanding of the en echelon offsets between flank structures, fold thrust mechanisms associated with tightening of fold hinges, and the extent to which basement offset is a controlling factor in deformation. My work continues this analysis by testing previous hypotheses proposed by these studies.

Willis, J. J., and Groshong, R. H., Jr., 1993,
Deformation style of the Wind River Uplift and
associated flank structures, Wyoming, p. 337.

Figure 6: Crowd structures forming as a result of space constrictions during increased fold tightening and formation (after Brown, 1984) from Willis and Groshong (1993) that depict fault formation as a result of out-of-the-syncline deformation (Brown, 1984). Fault types shown above are similar to those that occur in the study area.

Rock Units

Rock units within the study area range from Precambrian to Quaternary in age. However, only rocks Triassic and younger are exposed. In this section, I define the lithology of the study area organized by their ability to form competent or incompetent packages, as well as by their general attributes which were ascertained from a number of sources (Ahlstrand, 1978; Antweiler et al.,1980; Bell and Middleton, 1978; Boyd, 1993; Curry, 1990; Goodell, 1962; Haun and Barlow, 1962; Picard, 1978; Winn and Smithwick, 1980) and my field observations. It is important to establish an early understanding of how the stratigraphy influences structural competencies, because competency directly influences on how packages deformed and dissipate stresses that produced the HDFL. Sequences of units such as limestones, sandstones, and dolomites tend to produce a competent package that tends to undergo flexural slip and will deform brittlely. These rock packages most commonly contain fractures used for analysis in this study. In contrast, shales or weakly consolidated siliclastic units that are interlayered within a stronger units tend to form a structurally incompetent packages and contain few fractures. However, because incompetent packages can undergo internal deformation, they can vary in thickness to accommodate any space constrictions that occur in the stratigraphy as a result of deformation. For a simplified stratigraphic column of the study area, see Table 1 below.

Love, J. D., and Christiansen, A. C., 1980, Preliminary correlation of stratigraphic units used on 1 and 2 degree geologic quadrangle maps of Wyoming: Wyoming Geological Association Guidebook, Annual Field Conference, v. 31, p. 279-282.

Table 1: Simplified stratigraphic column of the study area including units shown in cross section (Love and Christenson (1980).

Precambrian and Paleozoic

The Precambrian basement and the Cambrian Flathead (~250 ft) form a competent package that acts as the forcing member beneath the fold line. Field notes taken from the core of Sweet Water Anticline (Fig. 4) by Abercrombie (1989) indicate that the Precambrian basement is composed of migmatites, schists, and granites, that are crosscut by granitic dikes. The Cambrian Flathead sandstone sits unconformably atop of the basement, and is a reddish-pink quartz sandstone which has been slightly hardened.

The Cambrian Gros Venture Formation (~700 ft) forms the first incompetent package in the sequence, and is composed of green, glauconitic shales that are interbedded with slabby lenses of quartz sandstone.

The Cambrian Gallatin Limestone (~275 ft), Ordovician Bighorn Dolomite (~150 ft), and Mississippian Madison Limestone (~400 ft) form the second structurally competent package in the sequence. The Gallatin Limestone is composed of interlayered limestone and dolomite, while the Ordovician Bighorn Dolomite is composed of a hard, tan-brown-gray, siliceous dolomite. A major unconformity between the Bighorn and the Mississippian Madison Limestone formed during a period of erosion between the Ordovician and the Mississippian. The Madison Limestone is a blue-gray limestone rich in fossil content, that are commonly preserved within layers of chert.

The Mississippian/Pennsylvanian Amsden Formation (~150 ft) creates the second structurally incompetent package in the sequence. The Amsden is a reddish-brown cross bedded sandstone which is overlain by interbedded reddish shale and limestone.

The Pennsylvanian Tensleep Sandstone (~400 ft) and Permian Park City/ Phosphoria Formation (~250 ft) form the third structurally competent package in the sequence. The Tensleep is composed of a buff, mature, fine- to course-grained, friable sandstone which is very porous. It is a regional producer of oil and natural gas. The Tensleep is overlain by the Park City/Phosphoria Formation, which is a buff, slightly dolomitized limestone mixed with a variety of mudstones, cherts, and two thinly layered phosphate units.

Mesozoic

The Triassic Dinwoody (~60 ft) and Chugwater Group, which is composed of the Triassic Red Peak (~900 ft), Triassic Alcova (~10 ft), and Triassic Crow Mountain/Popo Agie (~100 ft) Formations, form a large incompetent package, despite having several highly competent zones. The Dinwoody Formation is composed of reddish siltstones, buff, slightly dolomitized sandstones, and greenish shales. The Triassic Red Peak Formation, which is the first formation that is exposed in the study area, sits atop the Dinwoody and is a hematite-stained, fine grained, red sandstone that is interbedded with shales. The Triassic Alcova Formation sits atop the Red Peak Formation, and is a thinly bedded, gray, micritic limestone. The Alcova Formation is strongly resistant to weathering and erosion, is a highly competent unit, and thus provides a large amount of fracture data for analysis. The Triassic Crow Mountain/Popo Agie Formations are mapped together in the study area due to gradational contact. The Crow Mountain Formation is a hematite-stained reddish siltstone that is overlain by the Popo Agie Formation, which is a mixture of purple-red siltstone and fine grained sandstone. The uppermost beds of the Popo Agie formation contain an ocher yellow claystone and interbedded calcareous accretions. The upper contact between the Popo Agie and Jurassic Nugget Sandstones are easily identifiable in field studies.

The Upper Triassic/Lower Jurassic Nugget Sandstone (~470 ft) forms the next structurally competent package. It is separable into three distinct units. The first unit is largely composed of hematite-stained siltstone with some interbedded sandstones. The middle unit is composed of very friable, fine grained sandstone that is a weak valley former. The upper unit is composed of friable, pink-buff and orange fine-grained sandstones that form hogbacks on the fold limbs. The Nugget Sandstone contains many fracture sets throughout the study area, and is an important source for my fracture analysis.

The Nugget Sandstone grades into Jurassic Gypsum Spring Formation (~175 ft), which is composed of interbedded hematite-stained siltstones, gypsum layers, and four very resistive limestone layers. The limestone layers range from one to four feet in thickness, and are useful when detecting deformation within the overall formation. Because the Gypsum Spring Formation is largely dominated by siltstones and gypsum, it is a structurally incompetent package between the Nugget and the overlying Jurassic Sundance Formation.

The Jurassic Sundance (~250 ft) and the upper Jurassic/lower Cretaceous Morrison/Cloverly (~350 ft) form a structurally competent unit comprised mostly of sands. The Sundance Formation contains a basal transgressive sequence which is identified by yellow-brown rip up clasts interbedded in a slightly dolomitic siltstone. The lower unit of the Sundance Formation is a reddish siltstone that is overlain by the upper unit, which is composed of an interbedded mixture of greenish, glauconitic sandstones and limestones. In northern portions of the study area, the Sundance Formation contains a large amount of shell hash that are not present in the southern portion. The Morrison/Cloverly Formations are grouped in the study area due to a very gradational contact nearly impossible to locate.

The Mesozoic strata ends with the structurally incompetent package of the Cretaceous Thermopolis (~150 ft), Muddy Sandstone (~30-50 ft), Mowry (~500 ft), Frontier (~1000 ft), and Cody Formations. The base of the Thermopolis formation is defined by the exposure of a rust-colored sandstone unit. The Thermopolis then grades into silts and sands of various color, and is capped near the top by brown and black shales, which are recognized at outcrop scale. The Muddy Sandstone sits atop the Thermopolis Formation along a very sharp contact, and is defined as a hard, fine to medium grained dirty sandstone with phosphatic grains. The Muddy Sandstone is one of the most recognizable in the sequence, as it lies between the shale-derived slopes of the Thermopolis and Mowry Formations. The Mowry Formation is a thick formation of interbedded gray shales and bentonite-rich siltstones. Weathered slopes of the Mowry are recognized by vegetation bands due to the bentonite concentrations, and makes it very easy to locate on aerial photographs. The Mowry Formation acts to dissipate fault offsets throughout most of the study area through internal deformation. The Cretaceous Frontier Formation is comprised of dirty orange sandstone layer interbedded with fossil-rich silts and shales. The contact between the Mowry and Frontier Formations is very difficult to determine based on its gradational nature. For this study, I defined the contact as the first thickly bedded, lithic quartz sandstone above the Mowry shales. There was additional difficulty when defining the contact between the Frontier and Cody Formations, as this too is a very gradational contact. However, I defined the contact by recognizing the onset of the Cody's badland-type topography, wherever it was exposed.

Cenozoic

The Undifferentiated Miocene conglomerates were identified in two locations within the study area: on terraces associated with the Little Popo Agie River near Dallas Dome's core area, and at the top of Table Mountain. The conglomerates include large cobble to boulder sized igneous and metamorphic rock within a fine-grained matrix.

Quaternary Alluvium deposits were identified along drainage patterns throughout the study area. Alluvium deposits were, in many cases, defined by nutrient rich soils making way for healthy green vegetation, and unconformable relationships with the underlying lithified formations.

CHAPTER II: DEFORMATION FEATURES AND HISTORY

Introduction

Deformation features observed within the study area are largely a result of regional horizontal stresses applied to a heterogeneous sedimentary sequence containing preexisting weaknesses and competency contrasts. However, complex local stress regimes may also occur in response to folding and to the possible presence of compartmentalized basement faulting. The purpose of this chapter is to describe the mapped geological and structural features within the study area, to provide a basis for interpreting: 1) the origin of fracture sets across the area and 2) the deformation mechanisms that produced Dallas Dome.

Methodology

Field Methods and Techniques

Data collection and geologic mapping were done simultaneously. Bedding orientations were obtained using the right hand rule for dip direction and angle using a Brunton compass. The compass was set with a magnetic declination of fourteen degrees east. Station locations were obtained using Garmin handheld GPS devices GPSMap60 CS and Vista Cx. Measurements were made at a consistent interval, and deviated from that interval only when deformation became complicated or intensified. In many portions of the study area, it was impossible to obtain measurements or observations, due to hazardous environments (cliffs, e.g.), because structures were covered by float, or because surfaces were so heavily eroded that measurements were considered unreliable. In addition, electromagnetic fields produced by powerlines, especially along the forelimb of Dallas Dome, locally created interference and accuracy issues with the Brunton Compass. Areas containing fracture data were measured to determine all possible joint sets preserved within that given area. Other information included in station descriptions were: lithologic descriptions and formation name at station, fracture descriptions, proximity to faults (where applicable), and confidence in measurements taken. Mapping was done on printed 1:12000 scale base maps. Where deformation intensity was greater, mapping scale was increased to 1:6000. Data recorded on maps included bedding orientations, contacts, and any existing faults.

Station-based Methods

Field data obtained during the day were later converted to digital format using computers at the University of Missouri Branson Field Laboratory. Field notes were transferred to computer using Microsoft Word. Bedding and fracture data were transferred to Microsoft Excel. Station locations were downloaded from handheld GPS devices onto National Geographic TOPO! software, which was then used to export station data as tab delimited text that could be entered into Microsoft Excel. Finally, station location data and bedding/fracture data were combined into one Excel file that could then be used to sort and filter data. Field maps were transferred to a paper base map of the Lander 7.5’ Quadrangle.

Post-Data Collection Methods

Excel files including station locations and bedding/fracture data were converted into Apple iWork Numbers spreadsheets for home-based analysis. After sorting and filtering data, worksheets were exported as tab delimited files which could be read by Pangea Scientific's Spheristat 2.2 application, which is a stereographic projection program capable of plotting and statistically analyzing a wide range of three-dimensional orientation data. Planar data, including bedding and fracture orientations were plotted as poles to planes. The plotted data were contoured for percent concentration to distinguish clusters representing the fracture data sets affecting the study area and to determine the geometry of south Hudson Dome and north Dallas Dome. The 1:24000 base map developed while at the University of Missouri Branson Field Laboratory was transferred to digital format using ESRI's ArcGIS 9.2 Desktop software. The 1:24000 digital map was constructed by using a TIF file of the Lander 7.5' Quadrangle in order to create shapefiles depicting contacts between formations. Bedding orientation and fault symbols were created by ESRI and inserted from a digital database. Cross sections were created using Adobe Creative Suite 3.

Major Deformation Features Identified from the Mapping

Mapping indicated that Dallas Dome is a strongly asymmetric, southwest verging, doubly plunging anticline, trending NW/SE, which is offset in a left stepping en echelon fashion from the adjacent part of Hudson Dome to the north

(Plate 1). Dallas Dome has a breached core of Mesozoic rock ranging from the Triassic Red Peak Formation to the Cretaceous Frontier Formation . Flat-lying Miocene undifferentiated and Quaternary Alluvium deposits locally overlie the breached core throughout much of the study area.

Dallas Dome is strongly asymmetrical towards it southern terminus, where the forelimb strata are overturned. Progressing towards its northern terminus, this asymmetry dissipates, as forelimb strata become less inclined. The backlimb of Dallas Dome, which dips into the adjacent Wind River Basin, remains consistent in its attitude from south to north termini, dipping between 15 and 25 degrees to the northeast.

Within the study area, four structural features were identified, and are briefly described here in order from most significant to least significant:

The forelimb fault (FLF) (Fig. 7i, ii - Box A) is a northeast dipping reverse fault with an inferred dip of 40 degrees (Plates 1-4). It is the most significant and continuous fault throughout the study area, and can be inferred where the Cretaceous Frontier formation sharply changes in attitude coming off the Wind River dip slope (WRDS) at 10 degrees, to a steep 75 to 90 degrees on the Dallas Dome forelimb.

The backlimb thrust (BLT) (Fig. 7i, iv - Box D) is a continuation of the backlimb thrust observed on Derby Dome by Brocka (2007). Brocka inferred the BLT to be steeply dipping, then shallowing until soling out into the Triassic Chugwater Group. Within the study area, it duplicates Cretaceous Muddy

Sandstone in the Lander SE 7.5’ Quadrangle. As the fault proceeds to the northwest, it migrates into the Mowry Shale, where it terminates.

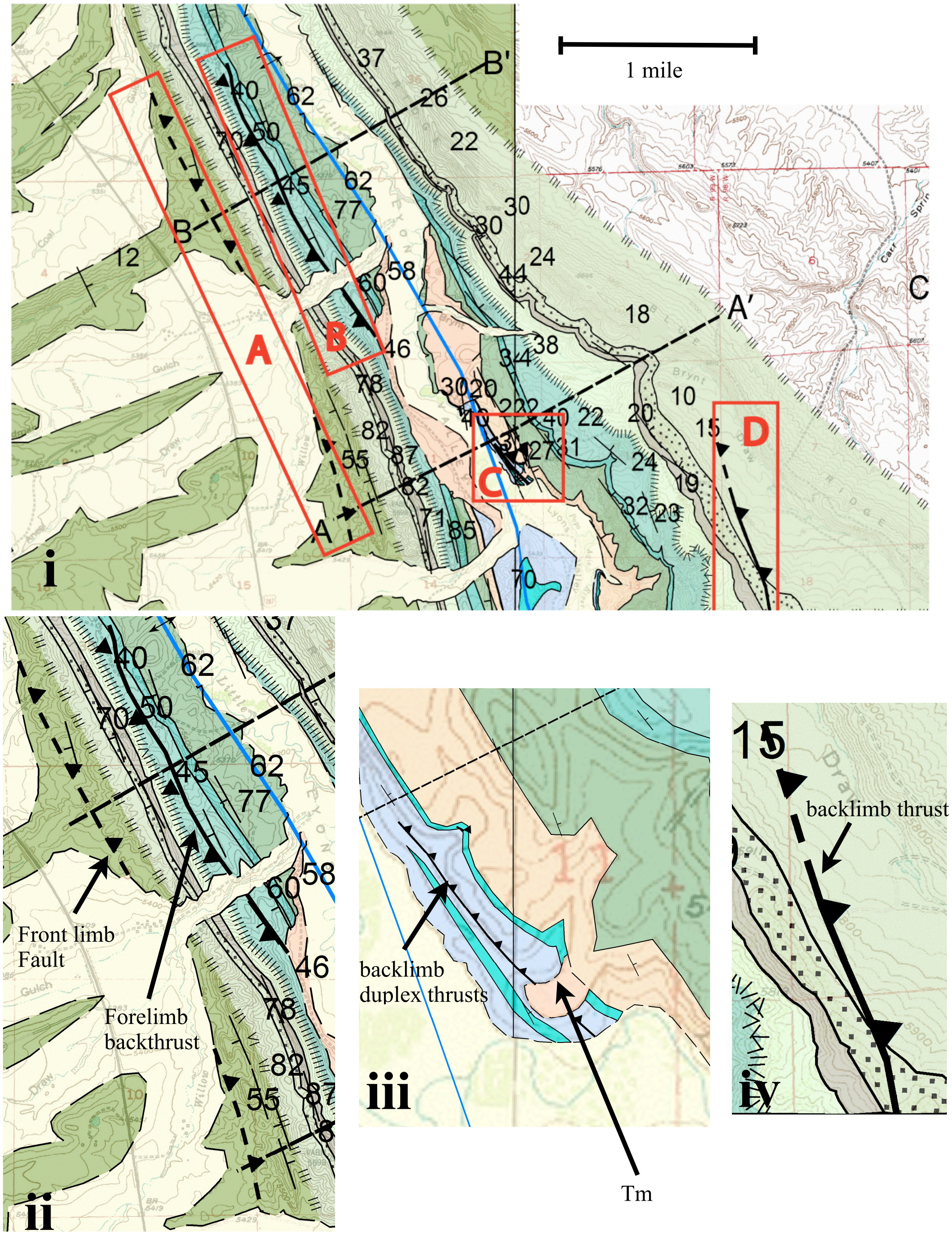

Figure 7i-iv: i) Rendering of Plate I showing the location of major deformation features in the study area. The FLF, FBT, BDTs, and BLT are contained within boxes A, B, C, and D, respectively. ii) Insets A and B combined to show FLF and FBT). iii) Inset C for BDTS. iv) Inset D for BLT. Tm represents Miocene undifferentiated sediments covering the fault.

The forelimb backthrust fault (FBT) is a high angle reverse fault (Fig. 7i, ii, Box B) that exists on the forelimb of Dallas Dome, and duplicates red units of the Jurassic Sundance Formation (Fig. 8). The fault progresses northward into the Jurassic Gypsum Spring formation, where it eventually terminates. The southern terminus of the FBT is not observed because it is covered by Miocene undifferentiated deposits.

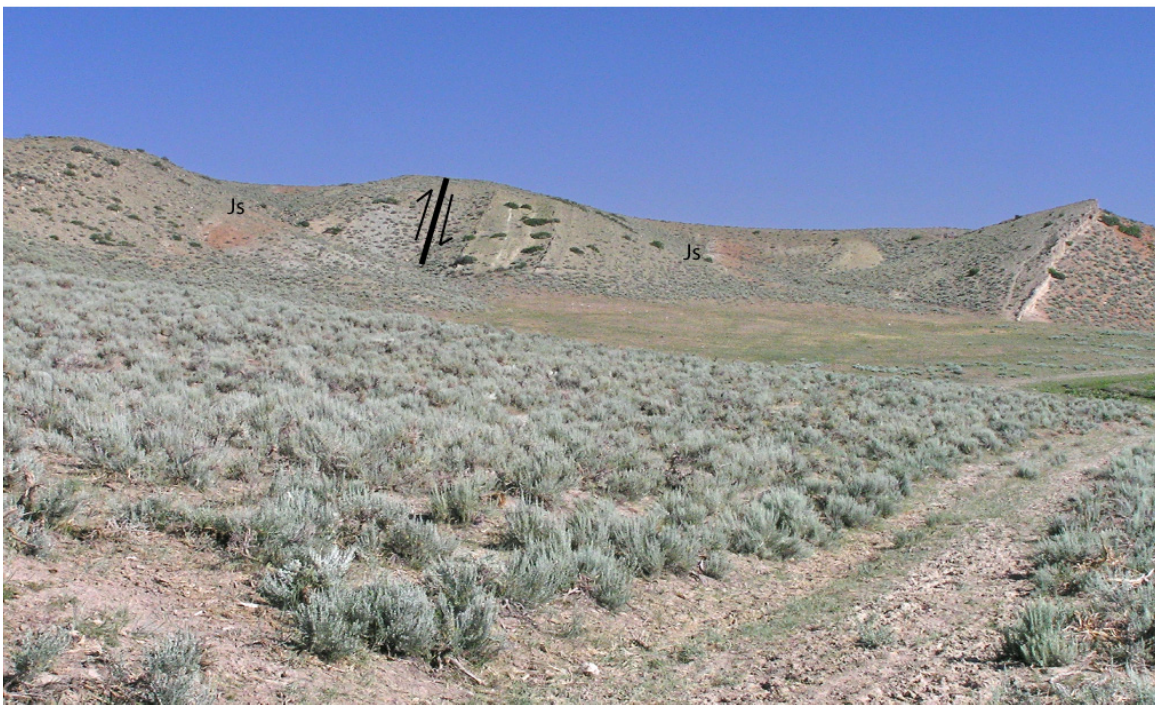

Figure 8: Photograph of the forelimb "backthrust" fault, viewed to the north. Undifferentiated Miocene deposits in the foreground obscure the southern terminus of the fault.

The backlimb duplex thrusts (BDTs) (Fig. 7i, iii, Box C) are a set of low angle thrust faults (~20 degrees) that duplicate Triassic Alcova limestone (Fig. 9). The fault's northern terminus occurs within the Triassic Red Peak formation near the nose of the fold. The southern terminus is covered by Quaternary alluvial deposits.

Figure 9: Photograph showing one of the backlimb thrusts (BDTs), viewed to the north.

Origin of the Major Deformation Features

Interpretations of the origin for each major deformation feature are constrained by surface mapping, field measurements, sparse well log information, and previous studies, and they are illustrated in cross sections AA', BB' and CC" (Plates 3, 4, and 5)

The geometry of Dallas Dome is strongly controlled by the FLF, which is interpreted to extend into the Precambrian basement (Plates 3-5). The FLF is interpreted to have a consistent dip of 40 degrees from the surface to the basement, based on fault geometries on the COCORP seismic image and location of the fault from well log data provided by the Wyoming Oil and Gas Conservation Commission (well #4901305576). Brocka (2007) observed the continuation of this fault to the southernmost extent of Dallas Dome, where it is accompanied by a parallel fault located 600 vertical feet above the FLF, referred to here as the Blind Reverse Fault (BRF). This interpretation is based on well log data from the Wyoming Oil and Natural Gas Conservation Commission (well log #4901305576). In addition, Brocka (2007) inferred this subsurface geology based on well log data from the Wyoming Oil and Natural Gas Conservation Commission (well log #1305420), and on his own surface measurements. He concluded that the offset along the FLF in the southern extent of Dallas Dome paled in comparison to the BRF.

The Blind Reverse Fault (BRF) dips 40 degrees to the northeast, and lies nearly 600 vertical feet above the FLF near the southern terminus of Dallas Dome. Near the southern extent of Dallas Dome, forelimb strata can be seen slightly overturned. As the fold progresses north, forelimb strata are restored to their normal, southwesterly dipping attitude, where bedding becomes increasingly shallow.

The formation of the BRF follows Berg's (1962) model for the formation of a dual thrust system, whereby the primary controlling fault, here the FLF, suffers sufficient offset such that forelimb strata are increasingly overturned, and a new fault develops and becomes the primary controlling fault (Fig. 10). The development of a dual thrust system forms can be viewed in three distinct stages: early, middle, and late. Early stages of formation involve rotation of the forelimb strata such that they approach overturning, and the new fault forms. Middle stages of development show that forelimb strata become slightly overturned and offset along the new fault becomes apparent. The final stage of development in the dual thrust system shows that forelimb strata are significantly overturned, and that the new fault has experienced such offset that it becomes the primary controlling fault in the dual thrust system.

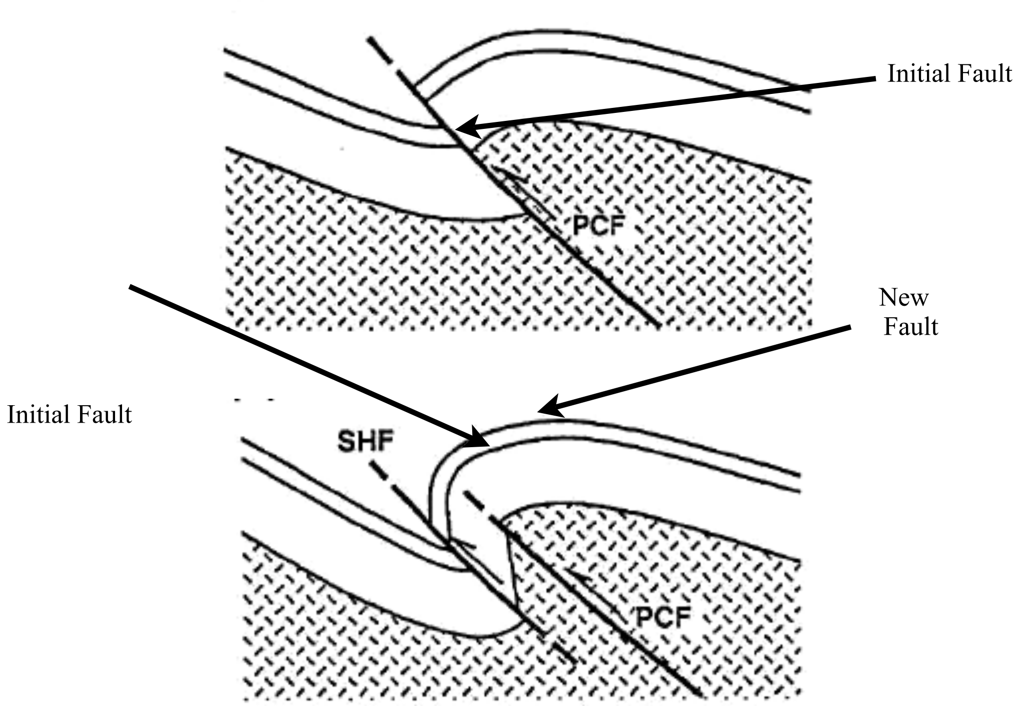

Figure 10: Early (top) and late (bottom) stages of evolution of the dual thrust model proposed by Berg (1962). Modified from Berg (1962).

Interpretations for both the FLF and BRF change significantly as the fold progresses towards its northern terminus. Near the southern extent of Dallas Dome, forelimb strata are nearly vertical, and supports the interpretation that evolution of the dual thrust system has reached the middle stage of development.

However, bedding returns to normal attitudes and becomes increasingly shallow towards the northern terminus of the fold form. This indicates that the dual thrust system becomes less evolved as the fold progresses north, and that the BRF becomes less significant. AA' illustrates FLF as the primary controlling fault, where the BRF has significant displacement but is not the dominant fault. Progressing north to AA', the BRF is illustrated as forming within the upper portion of the sedimentary sequence, and does not extend into the basement. As such, offset along the BRF diminishes to the north, such that north of BB', the BRF no longer appears. This is illustrated in CC', where the FLF is the primary controlling fault, and the BRF is no longer present.

The backlimb thrust (BLT) duplicates the Cretaceous Muddy Sandstone on the backlimb of Dallas Dome, and is a continuation of the backlimb thrust mapped by Brocka (2007). As the fault trace continues northwards, it cuts up section into incompetent layers of Mowry Shale, where it cannot be traced. While this feature is not contained within cross sections completed by this study, it is important to discuss why this feature occurs, and why it no longer continues. The BLT is interpreted to be a result of the progressive tilting of the backlimb of Dallas Dome. At some depth, the BLT forms as a detachment between units with high competency contrasts, which is most likely located within the Triassic Chugwater Group, where moderately competent sands are inter-layered with thick shales. The orientation of the BLT changes sharply as it approaches the surface, where it becomes very steep.

The BLT terminates shortly after cutting into the Mowry shale. Apparently, either the Mowry dissipates offset along the fault through internal deformation or the fault simply experiences a significant loss of displacement as it continues north from Brocka's study area, such that it is no longer expressed on the surface. The later interpretation seems more likely; since surface measurements in the Mowry do not indicate any internal deformation. The backlimb duplex thrusts (BDTs) that appear lower in the stratigraphic section, may have taken up displacement dissipated in the overlying BLT (see discussion below).

The forelimb backthrust (FBT) on the forelimb of Dallas Dome duplicates the Jurassic Sundance formation (Fig. 8). The southern terminus of the fault is covered by Miocene deposits, as there is no exposure of the fault to the south (Fig 7i, ii, Box B). The fault extends to the north where it cuts down section into the Jurassic Gypsum Spring formation, and eventually terminates. Formation of this fault is encouraged by the presence of the FLF and BRF, where the FLF cuts through the entire sedimentary sequence, and strata directly in front of the tip of the BRF are rotated such that they move from the hanging wall into the footwall. This may subsequently cause stresses parallel to bedding to concentrate within the sequence and become accommodated by slip along a detachment zone in relatively weak materials. The base of the Jurassic Sundance formation is primarily composed of weak silts and shales, such that faults may form and cut up-section

The backlimb duplex thrusts (BDTs) are a series of two low angle thrusts that duplicate the Triassic Alcova formation. These thrusts are located within the core of the dome, adjacent to the Little Popo Agie River. The lower thrust duplicates the Alcova with as much 70 feet of displacement, while the upper thrust has a displacement of about 10 feet. Both faults terminate to the north in the Triassic Chugwater Group near the nose of Dallas Dome. The southern terminus appears to be concealed by Quaternary alluvial deposits. Like the backlimb thrust (BLT), these faults form as a result of layer parallel shortening as backlimb strata are tilted, and detachments form between contrasting competencies within the Triassic Red Peak formation. It is apparent from geologic mapping that the BLF and BDTs share a geographical relationship, as the northern terminus of the BLF and northern terminus of the BDTs nearly overlap along strike. As displacement dissipates along the BLF towards its terminus, stresses associated with tilting are transferred to deeper levels of the section to create the BDTs,, which have continued displacement beyond the terminus of the BLF and propagated further north in the fold.

Relative Timing of Mapped Deformation Features

This section focuses on constraining the relative timing and order in which the mapped deformation features discussed above. Here, each feature will be discussed in chronological order, from first to last. This order is determine based on field observations, as well as by geographical and geological relationships with one another, and by geometric relationships inferred for the features at depth and shown in cross sections AA' and BB'.

The front limb fault (FLF) is interpreted to be equivalent to the basement controlling fault described by Berg (1962) in his dual fold thrust system for the Wind River uplift. As such, the FLF is believed to be a major early feature leading to the formation of Dallas Dome, and because of its relationships with other deformation features, this fault is the first to form among the observed features.

Soon after the FLF formed, the blind reverse fault (BRF), overlying the FLF formed due to over-tightening of the hinge of Dallas Dome.

There is no evidence to constrain the relative timing for the forelimb backthrust fault (FBF), the backlimb fault (BLF), or the backlimb duplex thrusts (BDTs). Based on geometric relationships between the FLB and BRF with the FBF, it can be inferred that the FBF formed later in the sequence, and sometime before the faults existing on the backlimb. However, this interpretation is highly speculative.

Based on interpretations made by Brocka (2007), tear faults within the basement, creating the left stepping en echelon style of the folds, do not affect the trend of the backlimb thrust. Thus, the backlimb fault is interpreted to have formed sometime after the FLF and BRF. Because the BDTs share a somewhat speculative relationship with the BLF, these faults are believed to have formed sometime after both basement involved faults. Relative timing between the BDTs and the BLF is speculative, but because the basement controlling fault has been interpreted to have originated southwest of the study area, and progressed towards the NW, it might be inferred that the BDTs formed after the BLF.

CHAPTER III: FRACTURE ANALYSIS AND DEFORMATION MECHANISMS

General Background

The previous chapter was devoted to introducing and describing the various deformation features, from the large scale folds to the small scale faults. This chapter will focus on using models and concepts derived from previous studies, along with my own data from this study, to interpret the progressive formation of these structural features and to deduce the mechanisms responsible for their formation.

Two end member folding mechanisms, buckle folding and forced folding, are the most likely mechanisms responsible for the formation of Laramide basin margin folds (Stearns, 1978; Cosgrove and Ameen, 2000; Brown, 1988). While each of these mechanisms is distinct, they may occur simultaneously during the folding process in response to the same regional stress regime (Cosgrove and Ameen, 2000). In Laramide foreland areas, forced folding models for the generation of basin margin folds are similar to the larger scale mechanisms that may drive Laramide mountain building (e.g. Berg, 1962). Forced folds were first described by Stearns (1978) as those that have a final shape and trend that are the same as the shape and trend of the forcing member below. Works by Brown

(1988) and Willis and Groshong (1993) have applied this concept to the formation of many of the features that occur in Laramide basin-margin folds (Fig. 6) which are the result of the forced fold mechanism. Progressive shear associated with offset along basement faults acting as the forcing members can also be modeled using trishear concepts first introduced by Erslev (1991) and later adapted by several other workers (e.g. Almendinger, 1998; Bump, 2003). Trishear modeling is a kinematic computer simulation model that calculates and illustrates the progressive strain developing within a triangular shear zone directly in front of a fault tip (cf. Erslev, 1991; Bump, 2003).

The second of the two end member hypotheses, buckle folding, occurs in response to layer-parallel shortening within a layered sequence. The shortening may be produced by regional tilting (e.g. uplift of an adjacent mountain range) or by large-scale regional stress regimes. In the study area, buckle folding and forced folding may occur simultaneously, since both involve responses to horizontal shortening. While previous workers (e.g. Willis and Groshong, 1993) attribute Laramide foreland deformation to forced folding, buckle folding in response to progressive tilting of the sedimentary cover rock (e.g. in response to uplift of the Wind River Mountains) may be an equally significant folding mechanism.

Because of the complexities that originate within basin margins, like those in the study area, the mechanisms leading to the formation of basin margin fold structures can be difficult to interpret. In order to make reasonable interpretations of structural features and their mechanisms of formation, it is important to further understand how buckle folds and forced folds are similar, and how they are different. The next section of this chapter introduces both end member models, and how fracture patterns can be used to suggest which end member mechanism is more significant within a given area. This relationship is the basis for the fracture analysis and interpretations for my study area.

<u>Buckle Folding versus Forced Folding</u>

Buckle Folding

Buckle folding is defined as a folding produced in response to instabilities occurring during layer-parallel shortening. In the study area, the deformation takes place within the sedimentary sequence with no involvement of basement rock in the associated deformation. Such folds tend to be periclinal in shape. That is, their aspect ratio, defined as the ratio of half the fold's wavelength to the hinge length, typically lies between 1:5 and 1:10 (Cosgrove and Ameen, 2000). In addition, buckle folds tend to die out very quickly in a profile scale, starting from the central area and progressing towards their ends (Cosgrove and Ameen, 2000).

Fracture generation during buckle folding can be regional and local in nature, and can occur before and during folding. Regionally derived fracture sets are commonly less complicated and tend to be more uniform as a result. Regional fracture sets commonly occur as extension joints that are normal to the least principal normal stress (σ_3) and contain the greatest principal stress (σ_1) in the plane of fracture. Such fractures commonly form perpendicular to the fold hingelines of concomitantly developing folds. Fractures derived from local stress fields, in contrast, are far more complicated and far less uniform, as they are bound to the formation of local structures and not to the regional stress orientations.

The relationship between regional and local stress-induced fracture sets is similar to the relationship between extensional and shear fracture sets formed during buckle folding. That is, extensional fracture sets are far less complicated and more uniform than shear fracture sets, as a result of uniform stress regimes. Extensional fracture sets are commonly characterized by steep dip angles and may strike parallel and perpendicular to the fold hinges in response to stresses produced during the folding process. For instance, those fractures forming perpendicular to the fold hinge, tend to be the result of extensional stresses derived from bending of the sedimentary sequence. Twiss and Moores (2007) discuss experiments by Curie and others (1962) that illustrate the stress field produced in response to buckling of a photo-elastic gelatin bar positioned such that its length is normal the least principal imposed stress (Fig. 11a). During folding, extensional fracture set B forms subparallel with the fold hinge, as a result of local concentrations of extensional stress on the convex side of the fold (Fig. 11c). In contrast, extensional fractures striking perpendicular to the hinge line tend to form as a result of lateral expansion of the sedimentary sequence as layer parallel shortening occurs. The experiment also accounted for the formation of these fractures (set A), but indicate that they form prior to folding when bedding is parallel with the maximum principal stress (Fig. 11b). As such, it is difficult to determine the nature of such fractures, as they may be the result of localized stresses or regional stresses (Cosgrove and Ameen, 2000).

Currie, J. B., Patnode, H. W. and Trump, R. P., 1962, Development of folds in sedimentary strata: Geological Society of America Bulletin, v. 73, p. 655-674.

Figure 11: Stress distribution in a gelatin bar undergoing buckling by layer parallel shortening, including a schematic of the experiment (A), stress orientations in the bar prior to folding (B), and stress trajectories in the bar after folding (C). Solid lines indicate the greatest principal stress, while dashed lines indicate the least principal stress. The shaded area indicates where layer parallel principal stress is tensile. Fracture sets A through E are described in the text(after Currie and others, 1962).

Shear fracture sets formed during buckle folding are far more complicated and less uniform throughout the folded area that those formed by regional stresses alone. Regional stresses inducing buckle folding will inherently produce local stresses associated with the buckling of the layered sequence as well. In addition, a sequence undergoing buckling may experience layer parallel slip between layers that may alleviate stress within some layers, but magnify stress in others. Local stresses produced by folding typically form conjugate shear fractures that wrap around the pericline, since layer parallel slip in such a feature occurs in all directions (Fig. 12). Twiss and Moores (2007) recognized these fractures as sets A, C, and E (Fig. 11c), where A occurs just before folding, C forms during folding on the concave side of the fold, and E forms on the convex side of the fold. Fracture sets C and E occur as a result of compressive and extensional stress concentrations within the fold, respectively. In general, conjugate shear fractures may be used to determine the local σ_1 stress orientations related to their location on the fold. The acute bisector of a conjugate shear set gives this σ_1 orientation (Cosgrove and Ameen, 2000).

The formation of both extensional and conjugate shear fractures as discussed above will form in an ideal system where sedimentary rocks are statistically homogenous and have experienced no periods of deformation previous to folding. However, geologic settings conducive to these characteristics are uncommon, especially in the Western Cordillera of the United States, which has experienced several episodes of deformation. Studies by Bergbauer and Pollard (2004) determined that when preexisting weaknesses in the sequence are present, they tend to control the formation of new fracture sets throughout the area. As such, fracture orientations discussed by Stearns (1978) may only conform to an idealized setting.

Stearns, D. W., 1978, Faulting and forced folding in the Rocky Mountains foreland, in V. Matthews, Ed. Laramide Folding Associated with Basement Block Faulting in the Western United States. Geological Society of America Memoir 15.

Ramsay, J. G., 1967, Folding and fracturing of rocks: United States, 568 p.

Figure 12: Periclinal dome with associated fracture patterns that are characteristic of buckle folds (a) (Stearns, 1978). 1b and 1c illustrate local stress perturbations due to folding of the cover rock (Ramsay, 1967).

Forced Folding

Forced folds are folds whose “final overall shape and trend are dominated by some forcing member below” (Stearns, 1978). One of the most common forced fold settings is associated with the folding of the sedimentary cover overlying fault offset of a rigid basement material. Such folds will inherently exhibit different geometries depending on the amount of slip and the type of displacement on the basement fault. For example, folding resulting from normal dip-slip along a fault will be geometrically different from folding produced by reverse dip-slip along a similar fault. Since faults can extend for long distances, forced folds formed over long fault traces in underlying basement can have much higher aspect ratios than buckle folds (Cosgrove and Ameen, 2000). Additionally, the fracture patterns associated with forced folds will also be different as result of the nature of offset on the forcing member.

The profile geometry of forced folds strongly depends on the amount and sense (normal or reverse) of slip along the basement fault (e.g. Ameen 1988, 1992; Richard 1990, 1991; Richard and Krants, 1991; and Nino et al, 1988). In cases where the basement fault motion is reverse or reverse oblique dip slip, layer-parallel shortening produces buckle folding in the sedimentary cover as well as forced folding. In contrast, forced folds overlying normal dip-slip faults form by the draping of the strata across the fault. This process results in layer-parallel elongation and no associated buckle folding in the sedimentary sequence.

Fracture distributions associated with dip slip basement offset were studied experimentally by Ameen (1988) using wooden "basement" blocks, below a "sequence of strata" represented by layered wax of differing competencies. The layers were imprinted with strain marker grids along two orientations of the model: one in the profile section, and the other on the surface of the layers. The grid was used to show how strain within the layers changed during progressive fault offset. Results of the model showed that the cover deformed by both rigid body rotation and also by internal deformation (Cosgrove and Ameen, 2000). Both types of definition progressively decrease away from the location of basement offset towards the surface. Further analysis of the experiment indicated that the formation of strain fields and fractures associated with deformation are closely related to the sense of motion along the fault. For example, fracture patterns associated with normal faulting tend to be uniform throughout the fold as a result of relatively uniform extensional stresses that occur over the entire extent of the fold during progressive normal faulting (Fig. 13A). In contrast, fracture patterns associated with reverse faulting tend to be less uniform in both time and space. For instance, along some parts of the developing fold, local stresses may begin as compressional stresses but progressively change to extensional regimes as the fault offset and associated folding progress. As a result, fracture patterns associated with reverse faulting in the basement will change over time, and thus can create complex distribution of fractures in the folded area (Fig. 13B).

Cosgrove, J. W., and Ameen, M. S., 2000, A comparison of the geometry, spatial organization, and fracture patterns assocaited with forced folds and buckle folds: Geological Society Special Publications, v. 169, p. 7-21.

Figure 13: Forced folds and associated fracture patterns due to pure dip-slip reverse faulting (a) and pure dip-slip normal faulting (b) (Cosgrove and Ameen, 2000).

Methods: Fracture Analysis

Fracture orientations were collected and analyzed in three separate stages: 1) field collection, 2) digital conversion at the field station, and 3) fracture analysis while at the University of Missouri in Columbia. The three stages are described in the sections below.

Field Collection

Fracture orientations were collected from structurally competent formations during the field geologic mapping. Orientations were obtained using the Brunton GeoTransit compass. As a result, all information collected in the field was expressed as dip azimuth and inclination. Orientation data were transferred using a water-resistant field notebook, in addition to a digital voice recorder. Fracture orientations were collected as frequently as possible in order to obtain a large number of orientations within the dataset. In most locations only one orientation of each fracture set was recorded. However, in some cases larger numbers of one set were recorded to show the dominance of one set over another. All station locations containing fracture data were recorded as waypoints in UTM coordinates using Garmin handheld GPS receivers with an accuracy of ten meters or less.

Station Based Digital Conversions

After returning from the field to the University of Missouri Branson Field Laboratory in Sinks Canyon, orientation data were recorded into a Microsoft

Excel worksheet and converted to a form that would be accepted by Pangea Scientific's SpheriStat 2.2 analysis software. Dip azimuth measurements were converted to strike directions for the observed fractures by subtracting ninety degrees from the dip azimuth. This conversion reformats the data to fit the right-hand-down-dip rule for collecting strike and dips in the field. Station locations were downloaded from Garmin handheld GPS receivers used in the field, to the National Geographic TOPO! software application. Upon extraction, station locations were converted into a text file readable by Microsoft Excel. Station location worksheets and fracture orientation worksheets were combined to yield a single worksheet containing station number, station location in UTM coordinates, strike and dip of fracture sets, and from what rock formation the fracture sets were taken from at that location. Conjugate sets were noted where they were observed. However, in most cases it was difficult to decipher conjugate sets in a timely manner while in the field. Instead, most conjugate relationships were evaluated while at the University of Missouri in Columbia using the SpheriStat software application.

Fracture Analysis

Once back at the University of Missouri in Columbia, worksheets containing all pertinent data (e.g. location, orientation) were converted into a tab delimited text file in Microsoft Excel. Text files were uploaded into Pangea Scientific's SpheriStat version 2.2 software application for fracture analysis. After the initial analysis, orientation data compiled in the Microsoft Excel worksheets were separated by waypoint ranges into three location groups: 1) stations originating from the Wind River dip slope, 2) stations originating from the forelimb of Dallas Dome, and 3) stations originating from the backlimb of Dallas Dome. These three groups were subsequently compiled into three separate Microsoft Excel worksheets, and the data were exported as tab delimited text files that could be read by the Spheristat software application. Wind River dip slope fracture data were analyzed first in order to determine regional stress induced fractures that could not have been produced by local stresses associated with folding processes. Analysis of fracture sets within the forelimb and backlimb areas of Dallas Dome followed thereafter in order to determine fracture sets associated with fold generation and its mechanisms. All fracture sets were evaluated using stereographic projections and rose diagrams generated by Spheristat.

Results

This section is broken into two separate subsections. The first describes the results from the fracture analysis of each of the areas listed above. The second interprets the results of the analysis in the context of previous regional tectonic studies (Coney, 1978; Bird, 1998), and kinematic the models of Bird (1998).

Results

In addition to the three data regions noted above, data from the forelimb backthrust fault, as well as the backlimb duplex thrusts (duplicating the Triassic Alcova Limestone), were analyzed in order to determine the mechanisms of fracture generation in the vicinity of these structures. The order in which these features are discussed is: 1) the Wind River dip slope, 2) the Dallas Dome forelimb and associated faults, and 3) the Dallas Dome backlimb and associated faults.

The Wind River dip slope contains two prominent regional fracture sets, R1 and R2. (Fig. 14). R1, the most common of the three sets, has an azimuth of 45/235 degrees; and the R2 fracture set has a dominant azimuth of 85/265 degrees.

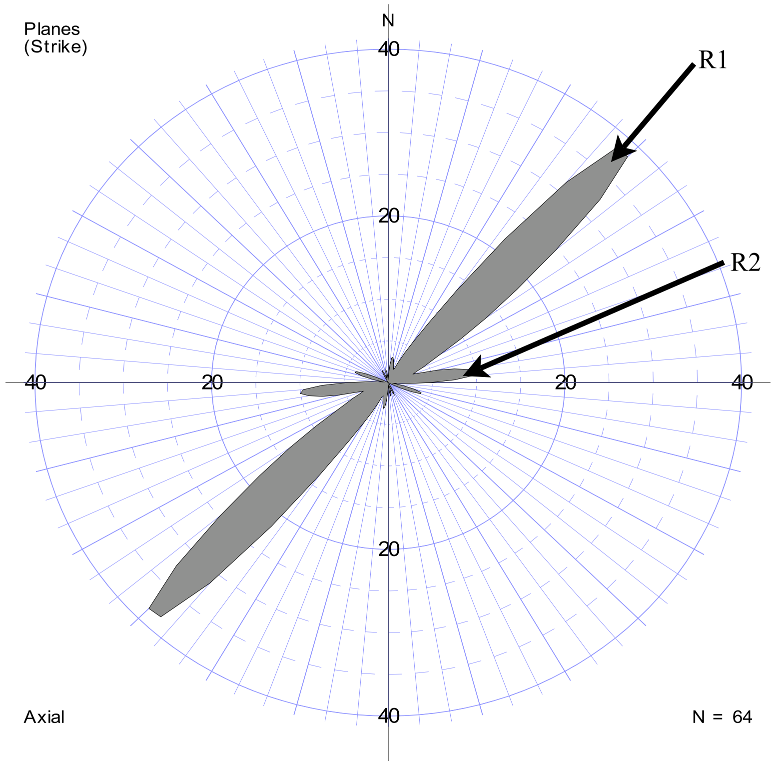

Counting Parameters

Number of Data Points in Set	53
Number of Data Points Included	52
Type of Data	Planes (Strike)
Range of Dip Angles	60° - 90°
Class interval	10°
Class Alignment	Start at 0°N
Kurtosis, k, of Smoothing Function	206
Half-width of Smoothing Function	±4.7°
Unweighted Calculation	

Frequency Statistics

Mode (Peak)	30.8%
Azimuth Range of Mode	40° - 50°
Smooth Peak	29.3%
Azimuth of Smooth Peak	42.5°
Expected Value, E	5.6%
Standard Deviation	4.7%
95% Confidence Level	>14.9%

The distribution has a preferred trend.

Figure 14: Rose diagram showing preferred joint orientations on the Wind River Dip Slope.

The Dallas Dome forelimb contains two additional fracture sets: J1, a highly dominant fracture set with an orientation of 65/244, and J2, a much less common set with an orientation of 150/330. Outcrops adjacent to the forelimb back-thrust fault on the Dallas Dome forelimb indicates similar fracture sets (Fig. 15).

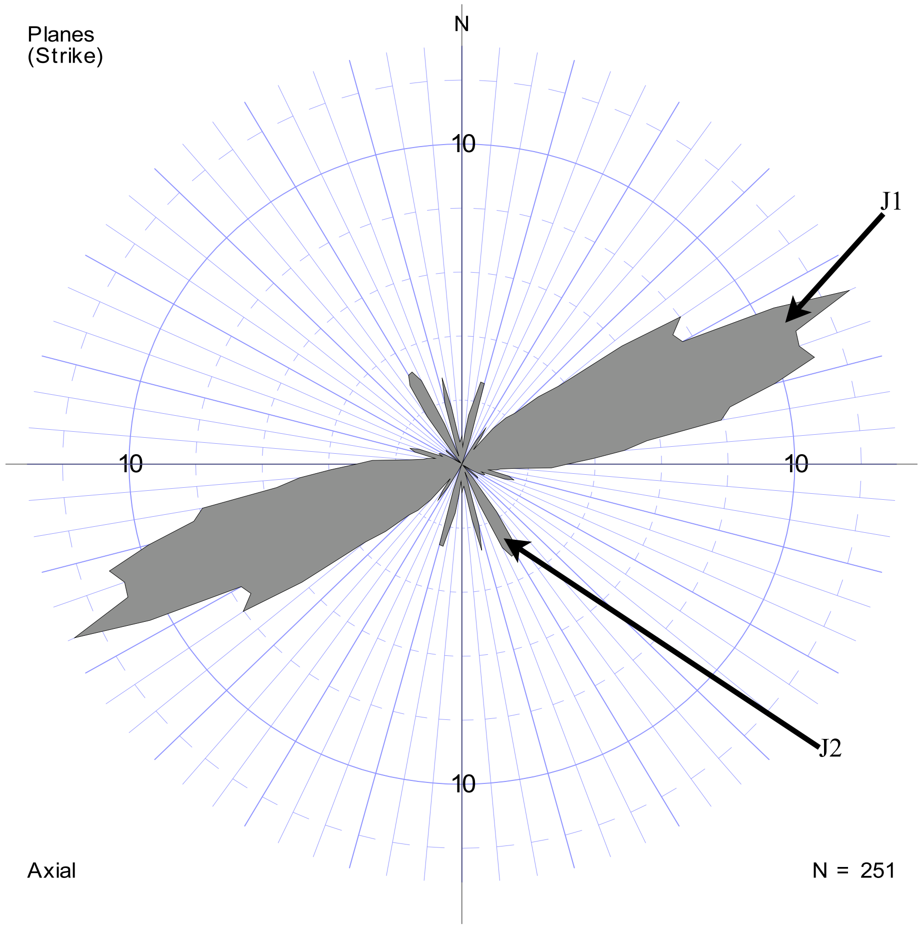

Counting Parameters

Number of Data Points in Set	251
Number of Data Points Included	179
Type of Data	Planes (Strike)
Range of Dip Angles	60° - 90°
Class interval	5°
Class Alignment	Start at 0°N
Kurtosis, k, of Smoothing Function	825
Half-width of Smoothing Function	±2.3°
Unweighted Calculation	

Frequency Statistics

Mode (Peak)	14.5%
Azimuth Range of Mode	70° - 75°
Smooth Peak	12.8%
Azimuth of Smooth Peak	65.0°
Expected Value, E	2.8%
Standard Deviation	1.8%
95% Confidence Level	>6.4%

The distribution has a preferred trend.

Figure 15: Rose diagram showing preferred orientations on the forelimb of Dallas Dome.

The Dallas Dome backlimb contains all fracture sets found within the Wind River dip slope and the Dallas Dome forelimb fracture analyses (Fig. 16).

Additional fracture sets found on the backlimb include J3 (110/290), and J4 conjugate set (60/240 and 75/255). J3 ranges widely in strike orientation. Dip angles for J3 also vary from 60-90-60. The J4 conjugate set forms around the J1 set, and are dominantly by large dip angles exceeding 75 degrees.

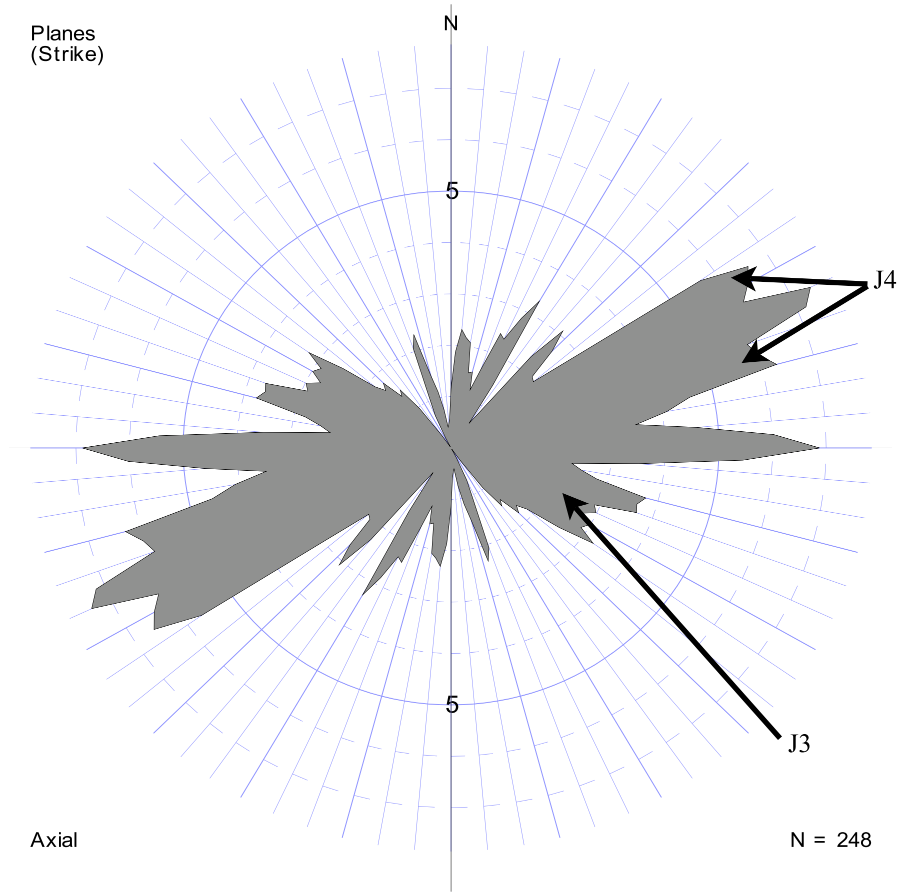

Counting Parameters

Number of Data Points in Set	248
Number of Data Points Included	230
Type of Data	Planes (Strike)
Range of Dip Angles	60° - 90°
Class interval	5°
Class Alignment	Start at 0°N
Kurtosis, k, of Smoothing Function	825
Half-width of Smoothing Function	±2.3°
Unweighted Calculation	

Frequency Statistics

Mode (Peak)	8.3%
Azimuth Range of Mode	65° - 70°
Smooth Peak	7.8%
Azimuth of Smooth Peak	65.0°
Expected Value, E	2.8%
Standard Deviation	1.6%
95% Confidence Level	>6.0%

The distribution has a preferred trend.

Figure 16: Rose diagram showing preferred fracture orientations on the Dallas Dome backlimb.

<u>Interpretations</u>

Introduction

The overall objective of this study was to deduce the mechanisms of fold formation and their associated stress orientations. To develop a basis for comparison between my results from Dallas Dome and previous work, this section considers: 1) previous studies of regional stress patterns believed to be associated with the tectonic development of the Sevier and Laramide orogenies (Bird, 1998; Coney, 1978), and 2) fold-induced stress patterns (Ameen, 1990; Cosgrove and Ameen, 2000; Twiss and Moores, 2007), associated with buckle and forced folding.

Regional Stress Patterns

Regional stress orientations during the Sevier and Laramide orogenies have been studied using several methodologies, including: paleomagnetic studies, stress and strain indicators, and fault offsets (Willis and Groshong, 1993; Groshong et al., 1978; Brown et al., 1981; Brown, 1988; McElhnny and Lock, 1995; Van Alstine and de Boer, 1978). Bird (1998) compiled available data from such studies to produce kinematic models for maximum principal shortening directions during Sevier and Laramide times (Fig. 17a-c). He also produced kinematic models for the stress fields created during rotation of the Colorado Plateau. Bird concluded from his results that the mean principal shortening direction for the Sevier Orogeny was approximately E-W (90/270), while during the Laramide Orogeny, the principal shortening direction had changed to a NE-SW orientation (40/220).

Bird, P., 1998, Kinematic history of the Laramide Orogeny in latitudes 35 degrees - 49 degrees N, Western United States: Tectonics, v. 17, no. 5, p. 780.

Figure 17a-c: kinematic model results developed by Bird (1998) showing the progressive change in mean shortening direction from Sevier orogeny (A) to Laramide orogeny (C).

Coney (1978) completed vector analyses for Sevier and Laramide Orogenies using plate motions between Farallon and North American Plates to deduce convergence velocities. Coney concluded that from 155-80 m.y. (Sevier Orogeny), the two plates converged at a rate of 8cm/yr along an azimuth of 75 degrees; and from 80-40 my (Laramide Orogeny), plate convergence occurred at a rate of 14 cm/yr along an azimuth of 45 degrees.

The regional joint sets identified by my study are consistent with both these previous studies. R1(45/235) is the dominant regional fracture set located within the study area, and subparallel with the maximum principal stress orientation proposed by Bird (1998) (40 degrees) for the Laramide Orogeny, and subparallel with the convergence direction given by Coney (45 degrees). R1 is therefore interpreted to be a result of Laramide regional shortening during which the Farallon Plate subducted shallowly beneath the North American Plate at a rate of 14 cm/yr. R2 (85/255), the second most prominent regional fracture set in the study area, is oriented subparallel to the mean shortening direction and convergence direction proposed by Bird (1998) (90 degrees) and Coney (1978) (75 degrees) for the Sevier Orogeny, respectively. R2 is therefore interpreted to have formed as a result of stress fields generated during the Sevier Orogeny. Based on this interpretation, R1 is younger than R2.

Fold-Induced Fracture Patterns

Fold-induced fracture sets have been studied extensively by several workers (Ameen, 1988; Cosgrove and Ameen, 2000; Bergbauer and Pollard, 2004; Stearns, 1978; etc.). Generation of fracture sets within a sequence may form from one of two mechanisms: buckle folding and forced folding. In buckle folding mechanisms, fractures are generated by layer parallel slip. Two of the most common fracture sets induced by buckle folding are extensional and conjugate shear fracture sets that form with preferred orientations relative to the fold's hinge line (Cosgrove and Ameen, 2000). The extensional fractures occur both perpendicular and parallel to the hinge line but do not reflect regional stress orientations (Cosgrove and Ameen, 2000). Conjugate shear fractures formed from buckle folding are typically more complex than extensional fractures, as the geometries of conjugate shear sets vary based on their geographic location along the fold. In regards to forced folding, both extensional and conjugate shear fracture sets may form, though the latter is much more common. Conjugate shear sets forming as a result of forced folding are typically oriented such that their geometries indicate vertical uplift, which is one component of offset on dip-slip faults (Cosgrove and Ameen, 2000). These fracture sets also tend to strike sub-parallel to the fold hinge, a characteristic similar to extensional fractures associated with bending stresses during buckle folding. In a forced fold setting, conjugate shear fractures may be oriented such that their acute bisector is normal to the hinge line of the fold, while maintaining high dip angles (see Fig. 13 and previous discussion). These fracture sets are similar to those formed during buckle folding. However, because conjugate shear fractures sub-perpendicular to the hinge line in forced fold settings are not greatly affected by their spatial relationship to the fold, they tend to be more uniform.

Fold induced fracture sets observed within the study area include J1 (65/245), J2 (150/330), J3 (110/290), and J4 (60/240 & 75/255). J1 is an extensional fracture set that forms sub-perpendicular to the fold hinge of Dallas Dome. As such, J1 is interpreted to be the result of buckle folding. J2 strikes sub-parallel to the fold hinge of Dallas Dome with variable dip angles consistent with a conjugate shear set bisected by an associated extensional fracture set. As such, J2 could be associated with either buckle or forced folding. J3 is a conjugate shear set whose dip values range from 60-90-60 and is indicative of vertical stresses associated with forced folding. However, the orientation of J3 with respect to the hingeline of Dallas Dome is not consistent with either forced folding or buckle folding models. Thus, the origin of this fracture set is unclear. Finally, J4 is a conjugate fracture set that is subparallel to normal faults that occur in the southern part of the study area, near the interchange with Derby Dome, and are interpreted as a response to extension associated with the en echelon interchange between Derby and Dallas Domes.

CHAPTER IV: SUMMARY AND CONCLUSIONS

Fold forms occurring along the northeastern basin margin of the Wind River Mountains in west central Wyoming form ultimately as a result of regional tectonic stresses associated with uplift of the mountain range. Locally derived basement involved faulting formed as a result of over-tightening of the backlimb of the Wind River uplift, which led to high amounts of buckle folding within the sedimentary cover. Layer parallel shortening experienced during buckling induced the formation of several thrust features such that crowding could be accommodated. The study area was evaluated to determine to what degree this deformation was a result of forced folding versus buckle folding.

This study utilized a combination of surface mapping, fracture analyses, and fault/fold analyses in order to test previous hypotheses regarding these fold forms' formation and the stresses that produced them. The study was conducted in order to: 1) determine whether forced folding, associated with local basement faulting, affected the domes, 2) determine to what degree buckle folding, associated with regional stresses, produced the domes and their features, and 3) evaluate the degree to which local and regional stresses contributed to the folding process and to the interchange between Dallas and Hudson Domes. In order to address these topics, several objectives for this study were set. This section restates each objective and summarizes conclusions that were obtained while pursuing these objectives.

The first objective of this study was to map the distribution of rock formations and deformation features contained within the Lander 7.5' Quadrangle and adjacent areas, which contain the majority of Dallas Dome and the adjacent interchange with Hudson Dome to the north. From this objective, the following conclusions were made:

1) Dallas Dome hosts four major deformation features, including the front limb reverse fault, the backlimb thrust, the forelimb backthrust, and the backlimb duplex thrusts, in addition to the blind reverse fault illustrated on cross sections AA' and BB' (Plates 2 and 3). The geometry of Dallas Dome is strongly controlled by the front limb fault, a reverse fault with a 40 degree dip to the northeast. In the southern portion of Dallas Dome, the front limb fault is accompanied by a basement reverse fault, which parallels the front limb reverse fault and lies 600 vertical feet above the front limb fault. Formation of the blind reverse fault results in a dual thrust wedge, and occurs as a result of slight overturning of forelimb strata. The basement reverse fault suffers significant displacement near the southern portion of the fold, but diminishes towards the north, as forelimb strata shallow in dip. The backlimb thrust and backlimb duplex thrusts form as a result of tilting and layer parallel slip of backlimb strata, in order to accommodate crowding. A small forelimb backthrust fault (shown on Plate 3) occurs on the forelimb formed as a result of layer-parallel shortening and counterclockwise rotation on the steepening forelimb of the fold.

The second objective was to collect fault and fracture orientation data within the study area. The following conclusions were made regarding this objective:

2) The Wind River dip slope contained three regional fracture sets, R1 (45/225), R2 (85/175), and R3 (25/205). The forelimb of Dallas Dome contained fracture sets J1 (60/240) and J2 (160/340). The backlimb contained R1, R2, R3, J1 and J2 fracture sets, with additional sets J3 (105/285) and J4 (55/235 and 65/245).

The third objective was to determine how the fault and fracture data are related to the mechanics of formation of Dallas and Hudson Domes. The following conclusions were made regarding this objective:

3) R1 and R2 are regional fracture sets produced in response to the maximum maximum principal stress conditions during the Laramide orogeny, Sevier orogeny, and rotation of the Colorado Plateau, respectively.
4) J1, J2, J3, and J4 are fold induced fracture sets produced by local stress fields. J1 is an extensional fracture set associated with buckle folding. J2 is a conjugate fracture set bisected by an associated extensional fracture set, and may be associated with either buckle or forced folding. J3 is a conjugate shear set whose orientation reflects vertical stresses associated with forced folding, but is not observed in

either forced fold or buckle fold models. Thus, the nature of J3 is unclear. J4 is a conjugate fracture set that is subparallel to normal faults that occur in the southern part of the study area, near the interchange with Derby Dome, and are interpreted as a response to extension associated with the en echelon interchange between Derby and Dallas Domes.

The fourth objective was to determine whether the data and interpretations from Hudson and Dallas Domes are consistent observations and interpretations of Brocka (2007) for Derby Dome and its interchange with Dallas Dome and Sheep Mountain. The following conclusions were made:

5) Data and interpretations produced during this study were somewhat consistent with observations and interpretations by Brocka (2007). Points not consistent between the two studies include orientations of joint sets associated with Laramide orogenic shortening and presence of Sevier stress fields (R2). J2 is not a fracture set associated with regional tectonism, as suggested by Brocka.

The fifth and final objective of this study was to evaluate whether the regional stress regimes inferred to have affected Hudson and Dallas Domes are consistent with those inferred for other similar Laramide structures associated with the broad region of the Laramide orogen. The following conclusions can be made for this objective:

6) Fracture analysis of Hudson and Dallas Domes indicates that regional stress regimes affecting the study area are consistent with those observed along other structures associated with the broad region of the Laramide orogeny. R1 and R2 are associated with the Laramide orogeny and Sevier Orogeny, respectively. These fracture sets were found to be within limits of mean principal shortening directions and maximum principal stress orientations inferred by Bird (1998) and Coney (1978).

Appendix A: Orientations taken throughout the extent of Dallas Dome and the southern extent of Hudson Dome. Orientations were obtained using the right thumb rule.

Stn	Easting	Northing	Strike	Dip Angle	Formation
1	691748	4740598	167	65	Jn
1	691748	4740598	168	58	Jn
2	691941	4740124	140	56	Jn
2	691941	4740124	153	68	Jgs
4	691637	4739898	145	20	Kms
6	691958	4740035	145	86	Jgs
8	692170	4739691	160	62	Jn
10	692362	4739379	150	60	Jn
12	692175	4741554	354	32	Kms
14	692327	4740837	340	36	Jm
18	691012	4741468	185	37	Kms
20	691235	4741622	187	32	Jm
21	691720	4743067	355	50	Kms
24	691694	4741969	340	29	Jgs
25	691687	4741982	315	24	Jgs
29	691920	4741807	355	35	Jm
30	691836	4741835	345	38	Js
31	694400	4739452	315	18	Kf
32	693895	4738882	320	50	Kms
34	693811	4738863	330	30	base Kt
35	693669	4738779	330	40	base Jm
38	689830	4746277	15	10	Kms
62	689515	4747823	335	22	base Kt
63	689563	4747795	330	20	base Kt

Stn	Easting	Northing	Strike	Dip Angle	Formation
66	689572	4747647	358	23	base Kt
72	691351	4743503	355	20	Km
73	691492	4743430	342	40	Kms
74	691506	4743371	340	38	Kms
75	691432	4743400	320	18	Kms
77	691182	4743509	210	10	Kms
78	691125	4743642	200	6	Kms
79	691143	4743681	280	10	Kms
80	691171	4743668	280	10	Kms
82	690543	4743416	170	30	Kf
83	689610	4745768	115	20	Kms
84	689800	4745827	95	15	Kms
85	689858	4745847	50	12	Kms
92	690316	4746245	320	10	Km
94	689900	4745251	190	10	Km
106	688297	4749537	340	35	Jn
107	688320	4749460	338	38	Jn
108	688355	4749409	340	36	Jn
109	688480	4749399	345	46	Jn
110	688477	4749443	342	46	Jn
111	688482	4749541	335	35	Jgs
114	688043	4749116	173	44	base Jn
115	688005	4749318	172	32	base Jn
116	687977	4749472	175	30	base Jn
119	687667	4749581	175	60	Js
124	688257	4748647	160	45	Ta
125	688161	4748594	165	46	base Jn
142	688886	4747257	95	18	base Jn
260	694257	4737734	327	44	top Js

Stn	Easting	Northing	Strike	Dip Angle	Formation
262	694062	4737620	330	40	Jn
263	693923	4737507	327	30	Ta
264	693825	4737423	183	30	Ta
266	693855	4737492	300	20	Trp
267	694006	4737387	335	26	Ta
268	694117	4737200	338	25	Ta
269	694190	4737110	330	28	fault
270	694221	4737073	75	65	fault
271	694291	4737205	330	42	Jn
272	693937	4736416	173	70	Jn
275	693765	4736343	165	71	Js
276	693688	4736392	173	74	Jm
277	693490	4736550	153	48	Kms
278	693655	4736668	173	68	Js
279	693394	4737332	157	44	Js
280	694224	4736994	335	28	Ta
281	694250	4737027	325	26	Ta
282	694309	4736869	326	32	Ta
283	694468	4737023	329	34	Jn
285	695102	4737146	307	20	Jm
286	695129	4737060	307	20	Jgs
287	695033	4736984	310	21	Jn
314	694131	4735813	164	70	Jn
315	694128	4735856	173	74	Jn
316	694108	4735883	175	60	Jn
317	694630	4736011	295	28	Ta
346	694195	4735700	168	71	Jn
347	694166	4735664	165	69	Jn
348	694285	4735401	154	77	Jn

Stn	Easting	Northing	Strike	Dip Angle	Formation
349	694260	4735398	163	70	Jn
350	694219	4735397	172	65	Jn
351	694184	4735396	159	73	Jn
352	692381	4738869	346	68	Js
353	692459	4738816	148	46	Js
354	692491	4738779	129	50	Js
355	692609	4738735	341	84	Js
356	692637	4738691	162	74	Js
357	692680	4738641	144	79	Js
358	692734	4738743	152	78	Jgs
359	692636	4738884	152	60	Jgs
360	692639	4738960	149	62	Jn
361	692518	4739087	145	68	Jn
362	692467	4739193	146	66	Jn
363	692424	4739178	164	66	Jgs
364	692344	4739121	161	80	Js
365	692391	4739032	146	83	Js
366	692399	4739021	152	86	Js
367	694051	4737609	333	30	base Jn
368	694062	4737591	334	34	base Jn
369	694123	4737523	331	34	Jn
370	694216	4737309	341	33	base Jn
371	694250	4737250	338	36	base Jn
372	694270	4737203	338	44	base Jn
373	694328	4737135	332	36	base Jn
374	694403	4737050	332	39	Jn
375	694450	4736967	323	30	Jn
376	694500	4736923	327	39	Jn
377	694530	4736895	332	34	Jn

Stn	Easting	Northing	Strike	Dip Angle	Formation
378	694559	4736869	323	31	Jn
379	694786	4737025	300	20	Jgs
380	694778	4737050	309	32	Jgs
381	694667	4737126	315	24	Js
382	694622	4737207	325	20	Js
383	694586	4737298	305	38	Js
384	694517	4737318	316	32	Js
385	694457	4737348	335	24	Jgs
386	694392	4737473	300	18	Js
387	694364	4737519	340	36	Js
388	694327	4737556	331	28	Jgs
389	694258	4737685	345	36	Jgs
390	694205	4737768	325	39	Jgs
391	693138	4738142	145	35	Js
392	693034	4738265	151	58	Js
393	693008	4738247	162	62	Js
394	692945	4738156	143	60	Js
395	693001	4738036	155	73	Js
396	693050	4738076	147	67	Js
397	693171	4738334	156	47	Js
398	693583	4736160	154	84	Kms
399	693562	4736232	170	85	Kms
400	693541	4736351	159	82	Kms
401	693524	4736373	169	76	Kms
402	693491	4736509	166	66	Kms
403	693401	4736683	160	50	Kms
404	693327	4736900	150	48	Kms
405	693310	4736937	156	49	Kms
406	693277	4737022	161	55	Kms

Stn	Easting	Northing	Strike	Dip Angle	Formation
407	693186	4737284	153	32	Kms
408	693148	4737380	167	32	Kms
409	693014	4737634	153	46	Kms
410	692956	4737730	165	37	Kms
411	692898	4737539	157	82	Km
412	692944	4737471	153	54	Km
413	692989	4737396	153	58	Km
414	693025	4737312	159	72	Km
415	693065	4737235	160	78	Km
416	693208	4736873	161	78	Km
417	693272	4736712	170	78	Km
418	693315	4736621	339	77	Km
418	693315	4736621	164	82	Km
419	693401	4736342	348	86	Km
420	693449	4736260	330	80	Km
421	693470	4736220	0	80	Km
422	693855	4735832	177	72	Jm
423	693706	4735784	161	80	Kms
424	693888	4734650	156	76	Kf
425	694147	4734630	195	80	Kms
426	694134	4734549	155	70	Kms
427	694207	4734559	163	50	Kms
428	694045	4734462	167	83	Km
429	691292	4741843	180	30	Js
430	691314	4742187	172	28	Jm
431	691074	4742143	189	25	Kms
432	691088	4742246	178	32	Kms
433	691059	4742372	190	52	Kms
434	691039	4742498	184	35	Kms

Stn	Easting	Northing	Strike	Dip Angle	Formation
435	691055	4742567	185	27	Kms
436	691056	4742678	182	28	Kms
437	691074	4742731	203	28	Kms
438	691099	4742800	172	25	Kms
439	691160	4742847	174	24	Kms
440	691229	4742959	170	22	Kms
441	691240	4743060	195	18	Kms
442	691216	4743146	200	14	Kms
443	691270	4743206	200	18	Kms
445	691380	4742972	214	9	Kt
446	691359	4742955	290	15	Kt
447	691335	4742929	233	19	Kt
448	691312	4742901	205	16	Kt
449	691239	4742746	186	23	Kt
450	691171	4742707	193	27	Kt
451	691315	4742495	196	20	Jm
452	691276	4742309	194	24	Jm
453	691288	4742202	204	24	Jm
454	691332	4742226	187	30	Js
455	691365	4742411	185	28	Js
456	691952	4741952	0	42	Jm
457	692083	4741916	350	30	Kms
458	692106	4741790	353	56	Kms
459	692126	4741701	352	59	Kms
460	692161	4741620	352	59	Kms
461	692263	4741338	344	36	Kms
462	692258	4741338	344	36	Kms
463	692403	4740949	343	42	Kms
464	692564	4740733	335	42	Kms

Stn	Easting	Northing	Strike	Dip Angle	Formation
465	692593	4740709	354	48	Kms
466	692746	4740498	315	33	Kms
467	692793	4740418	348	32	Kms
468	692817	4740332	343	28	Kms
469	692940	4740183	344	30	Kms
470	692991	4740091	334	34	Kms
471	693043	4740046	334	32	Kms
472	693271	4739677	332	26	Kms
473	693361	4739549	320	20	Kms
474	693482	4739418	332	17	Kms
475	693539	4739325	318	22	Kms
476	693643	4739212	335	38	Kms
477	693724	4739062	280	30	Kms
477	693724	4739062	300	18	Kms
478	693821	4738985	329	24	Kms
479	693930	4738816	327	30	Kms
480	694083	4738585	317	35	Kms
481	694139	4738496	323	33	Kms
482	694230	4738373	315	24	Kms
483	694425	4738319	310	20	Kms
484	694254	4738107	332	18	Kt
485	694133	4738106	327	50	Js
486	694144	4738166	325	60	Jm
487	694004	4738194	322	52	Js
488	693964	4738296	320	44	Js
489	693935	4738340	318	30	Js
490	693890	4738422	319	39	Js
491	693760	4738510	335	42	Jgs
492	693803	4738422	319	40	Jgs

Stn	Easting	Northing	Strike	Dip Angle	Formation
493	693833	4738373	335	38	Jgs
494	693894	4738292	330	40	Jgs
495	693921	4738213	325	44	Jgs
496	693975	4738178	330	44	Jgs
497	693992	4738118	335	36	Jgs
498	693855	4738166	327	36	Jn
499	693850	4738235	335	39	Jn
500	693823	4738581	342	42	Js
501	693784	4738629	315	30	Js
502	693771	4738707	337	46	Jm
503	693680	4738772	327	48	Jm
504	693700	4738802	322	42	Jm
505	693816	4738850	325	30	Kt
506	693814	4738907	328	40	Kt
507	693697	4738999	322	43	Kt
508	693589	4738990	305	48	Jm
509	693508	4739074	335	34	Jm
510	693418	4739181	326	40	Jm
511	693160	4739575	333	40	Jm
512	693158	4739574	312	38	Js
513	692980	4739651	327	46	Js
514	692731	4740002	335	37	base Jm
515	692664	4740107	318	28	Jm
516	692577	4740206	356	32	Jm
517	692498	4740417	356	32	base Js
518	692375	4740705	325	56	Jm
519	692306	4740823	309	37	Jm
521	686965	4736093	317	20	Kf
522	687687	4736712	317	12	Kf

Stn	Easting	Northing	Strike	Dip Angle	Formation
523	687616	4736485	335	14	Kf
524	687651	4736436	327	11	Kf
525	687626	4736454	322	10	Kf
526	687384	4739342	315	18	Kf
527	687305	4739394	334	14	Kf
528	687331	4739395	322	20	Kf
529	687086	4739330	320	13	Kf
530	686183	4739582	333	12	Kf
531	686146	4739711	322	10	Kf
532	686021	4739745	344	20	Kf
533	686457	4740852	310	16	Kf
533	686457	4740852	314	12	Kf
533	686457	4740852	330	12	Kf
534	685774	4740147	330	14	Kf
535	685927	4739792	320	24	Kf
535	685927	4739792	334	16	Kf
535	685927	4739792	335	14	Kf
535	685927	4739792	345	15	Kf
536	685900	4739766	327	10	Kf
536	685900	4739766	345	24	Kf
537	685895	4739839	343	10	Kf
538	685746	4739841	337	13	Kf
539	685670	4739828	327	10	Kf
539	685670	4739828	328	13	Kf
540	685644	4739880	327	12	Kf
541	685591	4740032	317	10	Kf
541	685591	4740032	322	8	Kf
542	685687	4740085	335	11	Kf
543	686652	4739302	300	17	Kf

Stn	Easting	Northing	Strike	Dip Angle	Formation
543	686652	4739302	305	12	Kf
544	686386	4739410	310	12	Kf
545	686502	4739198	315	10	Kf
546	686479	4739031	300	15	Kf
547	686607	4738445	315	10	Kf
548	686558	4738535	333	12	Kf
549	694341	4736825	330	34	Ta
550	694444	4736852	350	42	Tcp
551	692696	4737612	334	90	Kf
551	692696	4737612	154	90	Kf
552	692790	4737452	150	80	Kf
553	692822	4737366	155	78	Kf
554	692891	4737232	154	70	Kf
555	692925	4737183	155	72	Kf
556	692997	4737060	160	75	Kf
557	693035	4736973	165	84	Kf
558	693118	4736846	159	87	Kf
559	693168	4736717	342	84	Kf
560	693228	4736561	340	82	Kf
561	690842	4738354	304	10	Kf
561	690842	4738354	330	12	Kf
562	690647	4738222	335	12	Kf
564	693804	4737600	167	18	Ta
564	693804	4737600	193	28	Ta
564	693804	4737600	193	24	Ta
564	693804	4737600	199	22	Ta
565	693808	4737546	183	18	Ta
566	693814	4737453	170	30	Ta
567	693850	4737445	185	24	Trp

Stn	Easting	Northing	Strike	Dip Angle	Formation
568	693933	4737446	335	20	Trp
569	693954	4737424	322	28	Trp
570	693981	4737426	347	24	Ta
571	694012	4737369	343	20	Trp
572	694039	4737306	333	22	Trp
573	694120	4737195	320	23	Ta
575	694142	4737117	330	22	Ta
576	693870	4737181	167	30	Ta
577	693874	4737165	174	48	Ta
578	693885	4737130	172	34	Ta
579	693979	4736778	173	48	Ta
580	690751	4747605	357	19	Kf
581	690749	4747520	338	17	Kf
582	690743	4747415	345	18	Kf
583	690750	4747334	355	20	Kf
584	690765	4747207	353	15	Kf
585	690782	4747046	350	20	Kf
586	690808	4746897	355	16	Kf
587	690806	4746719	335	40	Kf
588	690875	4746585	4	30	Kf
589	690974	4746442	355	32	Kf
590	690955	4746258	347	32	Kf
591	690768	4745919	330	26	Kf
592	690592	4746389	320	30	Kf
592	690592	4746389	339	26	Kf
592	690592	4746389	343	30	Kf
593	690467	4746731	343	24	Kf
594	690364	4747070	337	34	Kf
594	690364	4747070	344	30	Kf

Stn	Easting	Northing	Strike	Dip Angle	Formation
595	690312	4747295	330	42	Kf
596	690406	4747443	353	20	Kf
597	690679	4747908	355	25	Kf
598	690625	4748593	346	22	Kf
599	689017	4747596	356	30	Jn
600	689103	4747722	350	31	Jn
601	689087	4747651	342	26	Jn
602	689102	4747595	348	28	Jn
603	689095	4747438	348	15	Jn
604	689170	4747476	3	20	Jgs
605	689385	4747632	355	32	Js
606	689375	4747558	352	34	Js
607	689399	4747447	348	32	Js
608	689430	4747299	352	28	Js
609	689502	4747328	348	31	Jm
610	689569	4747788	343	24	Kt
611	689464	4748093	346	20	Kt
612	689425	4748194	337	20	Kt
613	689397	4748298	355	28	Kt
614	689399	4748408	344	20	Kt
615	689361	4748508	332	26	Kt
616	689365	4748618	325	30	Kt
617	689330	4748732	323	20	Kt
618	695544	4736660	142	20	Jm
619	695540	4736586	335	18	Js
620	695487	4736641	333	21	Js
621	695489	4736401	332	21	Js
622	695438	4736467	334	18	Js
623	695375	4736508	314	21	Js

Stn	Easting	Northing	Strike	Dip Angle	Formation
624	695320	4736579	295	25	Jgs
625	695239	4736638	335	25	Jgs
626	695130	4736803	320	24	Jgs
627	695491	4736783	332	17	Jm
628	695771	4736999	300	14	Kms
629	695671	4737123	300	15	Kms
630	695591	4737197	315	14	Kms
632	695459	4737333	323	10	Kms
633	695426	4737857	295	20	Kms
635	695103	4737935	300	18	Kms
636	694882	4738014	295	20	Kms
638	694840	4738071	350	20	Kms
639	694441	4738233	300	14	Kf
642	694401	4736694	334	40	Ta
643	694415	4736657	334	30	Ta
644	694368	4736430	325	18	Trp
645	694378	4736298	330	16	Trp
646	694367	4736275	300	10	Trp
647	694357	4736227	250	4	Ta
650	694073	4736396	165	58	Ta
651	692144	4738956	150	45	Kms
652	692357	4738598	150	82	Kms
653	691973	4739310	154	30	Kms
654	691900	4739432	159	50	Kms
655	691716	4739727	155	40	Kms
656	691668	4739343	157	70	Kms

Appendix B: Joint orientations throughout the extent of Dallas and Hudson Domes. Specific areas that were sampled include the Dallas backlimb (DBL), Hudson backlimb (HBL), the Dallas/Hudson interchange (NTCHNG), the Dallas forelimb (DFL), and the Wind River Dip Slope (DPSLP).

Stn	Easting	Northing	Strike	Dip Angle	Formation	Area	Faulted
23	691672	4741552	320	76	Jn	DBL	
24	691694	4741969	90	78	Jgs	DBL	
24	691694	4741969	120	79	Jgs	DBL	
24	691694	4741969	180	79	Jgs	DBL	
24	691694	4741969	210	77	Jgs	DBL	
25	691687	4741982	90	78	Jgs	DBL	
25	691687	4741982	120	79	Jgs	DBL	
25	691687	4741982	180	79	Jgs	DBL	
25	691687	4741982	210	77	Jgs	DBL	
28	691921	4741876	240	80	Jm	DBL	
29	691920	4741807	355	35	Jm	DBL	
30	691836	4741835	80	85	Jm	DBL	
30	691836	4741835	250	82	Jm	DBL	
61	689492	4747853	105	77	Kt	HBL	
61	689492	4747853	185	69	Kt	HBL	
62	689515	4747823	60	80	Kt	HBL	
62	689515	4747823	193	70	Kt	HBL	
66	689572	4747647	95	73	Kt	HBL	
66	689572	4747647	95	89	Kt	HBL	
72	691351	4743503	110	80	Kms	NTCHNG	
72	691351	4743503	200	80	Kms	NTCHNG	
74	691506	4743371	30	80	Kms	DBL	
74	691506	4743371	110	60	Kms	DBL	

Stn	Easting	Northing	Strike	Dip Angle	Formation	Area	Faulted
93	690317	4746244	100	74	Km	HBL	
93	690317	4746244	190	74	Km	HBL	
107	688320	4749460	58	85	Jn	HBL	
109	688480	4749399	90	88	Jn	HBL	
110	688477	4749443	90	70	Jn	HBL	
110	688477	4749443	242	80	Jn	HBL	
111	688482	4749541	245	76	Jn	HBL	
111	688482	4749541	290	88	Jn	HBL	
112	688449	4749600	145	33	Jn	HBL	
112	688449	4749600	230	70	Jn	HBL	
112	688449	4749600	230	90	Jn	HBL	
112	688449	4749600	240	88	Jn	HBL	
112	688449	4749600	260	80	Jn	HBL	
113	688420	4749662	93	77	Jgs	HBL	
113	688420	4749662	215	70	Jgs	HBL	
114	688043	4749116	236	89	Jn	HFL	
116	687977	4749472	60	83	Jn	HFL	
265	693845	4737461	25	81	Trp	DBL	
265	693845	4737461	298	80	Trp	DBL	
273	693910	4736418	15	7	Jn	DFL	
273	693910	4736418	285	64	Jn	DFL	
273	693910	4736418	295	37	Jn	DFL	
278	693655	4736668	82	76	Js	DFL	
278	693655	4736668	270	68	Js	DFL	
283	694468	4737023	57	88	Jn	DBL	
283	694468	4737023	125	50	Jn	DBL	
283	694468	4737023	249	80	Jn	DBL	
283	694468	4737023	253	74	Jn	DBL	
283	694468	4737023	255	86	Jn	DBL	

Stn	Easting	Northing	Strike	Dip Angle	Formation	Area	Faulted
284	695078	4737208	10	83	Jn	DBL	
284	695078	4737208	28	85	Jn	DBL	
284	695078	4737208	132	80	Jn	DBL	
314	694131	4735813	44	37	Jn	DFL	
314	694131	4735813	68	90	Jn	DFL	
314	694131	4735813	78	84	Jn	DFL	
315	694128	4735856	80	40	Jn	DFL	
315	694128	4735856	270	18	Jn	DFL	
316	694108	4735883	15	44	Jn	DFL	
316	694108	4735883	270	76	Jn	DFL	
317	694630	4736011	195	71	Ta	DFL	
339	695078	4736432	58	86	Jn	DBL	
339	695078	4736432	60	85	Jn	DBL	
339	695078	4736432	79	78	Jn	DBL	
339	695078	4736432	90	85	Jn	DBL	
339	695078	4736432	99	69	Jn	DBL	
339	695078	4736432	100	67	Jn	DBL	
339	695078	4736432	105	86	Jn	DBL	
339	695078	4736432	271	89	Jn	DBL	
340	695059	4736455	4	84	Jn	DBL	
340	695059	4736455	87	75	Jn	DBL	
340	695059	4736455	87	76	Jn	DBL	
340	695059	4736455	90	68	Jn	DBL	
340	695059	4736455	90	74	Jn	DBL	
340	695059	4736455	93	76	Jn	DBL	
340	695059	4736455	100	75	Jn	DBL	
340	695059	4736455	105	72	Jn	DBL	
340	695059	4736455	106	81	Jn	DBL	
340	695059	4736455	115	85	Jn	DBL	

Stn	Easting	Northing	Strike	Dip Angle	Formation	Area	Faulted
340	695059	4736455	202	89	Jn	DBL	
341	694999	4736546	7	80	Jn	DBL	
341	694999	4736546	15	86	Jn	DBL	
341	694999	4736546	89	71	Jn	DBL	
341	694999	4736546	93	80	Jn	DBL	
341	694999	4736546	95	74	Jn	DBL	
341	694999	4736546	95	89	Jn	DBL	
341	694999	4736546	96	78	Jn	DBL	
341	694999	4736546	100	82	Jn	DBL	
341	694999	4736546	105	88	Jn	DBL	
341	694999	4736546	190	77	Jn	DBL	
341	694999	4736546	194	84	Jn	DBL	
341	694999	4736546	310	14	Jn	DBL	
341	694999	4736546	315	70	Jn	DBL	
342	695095	4736033	15	81	Tcp	DBL	
342	695095	4736033	109	89	Tcp	DBL	
342	695095	4736033	126	90	Tcp	DBL	
342	695095	4736033	143	72	Tcp	DBL	
342	695095	4736033	170	85	Tcp	DBL	
342	695095	4736033	284	87	Tcp	DBL	
342	695095	4736033	290	68	Tcp	DBL	
342	695095	4736033	300	89	Tcp	DBL	
343	695061	4736094	25	85	Tcp	DBL	
343	695061	4736094	29	80	Tcp	DBL	
343	695061	4736094	107	84	Tcp	DBL	
343	695061	4736094	125	80	Tcp	DBL	
343	695061	4736094	135	76	Tcp	DBL	
343	695061	4736094	140	64	Tcp	DBL	
343	695061	4736094	162	68	Tcp	DBL	

Stn	Easting	Northing	Strike	Dip Angle	Formation	Area	Faulted
343	695061	4736094	202	88	Tcp	DBL	
343	695061	4736094	207	84	Tcp	DBL	
343	695061	4736094	305	86	Tcp	DBL	
344	695028	4736093	22	76	Tcp	DBL	
344	695028	4736093	111	78	Tcp	DBL	
344	695028	4736093	111	89	Tcp	DBL	
344	695028	4736093	126	85	Tcp	DBL	
344	695028	4736093	134	74	Tcp	DBL	
344	695028	4736093	184	89	Tcp	DBL	
344	695028	4736093	186	88	Tcp	DBL	
344	695028	4736093	187	88	Tcp	DBL	
344	695028	4736093	205	86	Tcp	DBL	
344	695028	4736093	294	78	Tcp	DBL	
344	695028	4736093	295	84	Tcp	DBL	
344	695028	4736093	300	85	Tcp	DBL	
344	695028	4736093	301	81	Tcp	DBL	
344	695028	4736093	303	76	Tcp	DBL	
344	695028	4736093	305	85	Tcp	DBL	
345	695022	4736020	40	78	Ta	DBL	
345	695022	4736020	54	72	Ta	DBL	
345	695022	4736020	55	74	Ta	DBL	
345	695022	4736020	63	80	Ta	DBL	
345	695022	4736020	64	74	Ta	DBL	
345	695022	4736020	161	87	Ta	DBL	
345	695022	4736020	165	84	Ta	DBL	
345	695022	4736020	225	63	Ta	DBL	
345	695022	4736020	247	84	Ta	DBL	
345	695022	4736020	320	81	Ta	DBL	
345	695022	4736020	342	82	Ta	DBL	

Stn	Easting	Northing	Strike	Dip Angle	Formation	Area	Faulted
346	694195	4735700	53	61	Jn	DFL	
346	694195	4735700	80	59	Jn	DFL	
346	694195	4735700	94	77	Jn	DFL	
346	694195	4735700	97	60	Jn	DFL	
346	694195	4735700	255	90	Jn	DFL	
347	694166	4735664	58	44	Jn	DFL	
347	694166	4735664	70	54	Jn	DFL	
347	694166	4735664	73	49	Jn	DFL	
348	694285	4735401	83	60	Jn	DFL	
348	694285	4735401	87	54	Jn	DFL	
349	694260	4735398	60	21	Jn	DFL	
349	694260	4735398	60	61	Jn	DFL	
349	694260	4735398	73	67	Jn	DFL	
349	694260	4735398	150	6	Jn	DFL	
349	694260	4735398	250	78	Jn	DFL	
350	694219	4735397	54	45	Jn	DFL	
350	694219	4735397	74	62	Jn	DFL	
350	694219	4735397	74	74	Jn	DFL	
350	694219	4735397	78	69	Jn	DFL	
350	694219	4735397	85	66	Jn	DFL	
350	694219	4735397	99	65	Jn	DFL	
350	694219	4735397	328	18	Jn	DFL	
351	694184	4735396	46	58	Jn	DFL	
351	694184	4735396	76	70	Jn	DFL	
351	694184	4735396	267	87	Jn	DFL	
351	694184	4735396	327	88	Jn	DFL	
351	694184	4735396	347	62	Jn	DFL	
353	692459	4738816	14	68	Js	DFL	
353	692459	4738816	273	78	Js	DFL	y

Stn	Easting	Northing	Strike	Dip Angle	Formation	Area	Faulted
354	692491	4738779	48	86	Js	DFL	y
354	692491	4738779	232	75	Js	DFL	y
355	692609	4738735	259	76	Js	DFL	y
355	692609	4738735	264	78	Js	DFL	y
355	692609	4738735	267	75	Js	DFL	y
356	692637	4738691	71	82	Js	DFL	y
356	692637	4738691	225	56	Js	DFL	y
356	692637	4738691	237	68	Js	DFL	y
356	692637	4738691	254	78	Js	DFL	y
357	692680	4738641	49	46	Js	DFL	y
357	692680	4738641	57	64	Js	DFL	y
357	692680	4738641	216	41	Js	DFL	y
357	692680	4738641	229	46	Js	DFL	y
358	692734	4738743	235	80	Jgs	DFL	y
358	692734	4738743	243	66	Jgs	DFL	y
359	692636	4738884	248	44	Jgs	DFL	y
359	692636	4738884	310	60	Jgs	DFL	y
360	692639	4738960	59	90	Jn	DFL	y
360	692639	4738960	121	70	Jn	DFL	y
360	692639	4738960	180	49	Jn	DFL	y
360	692639	4738960	239	90	Jn	DFL	y
360	692639	4738960	252	58	Jn	DFL	y
360	692639	4738960	263	80	Jn	DFL	y
360	692639	4738960	289	66	Jn	DFL	y
361	692518	4739087	225	74	Jn	DFL	
361	692518	4739087	243	66	Jn	DFL	
361	692518	4739087	253	65	Jn	DFL	
362	692467	4739193	133	75	Jn	DFL	
362	692467	4739193	144	80	Jn	DFL	

Stn	Easting	Northing	Strike	Dip Angle	Formation	Area	Faulted
362	692467	4739193	233	70	Jn	DFL	
362	692467	4739193	242	78	Jn	DFL	
362	692467	4739193	247	66	Jn	DFL	
362	692467	4739193	251	61	Jn	DFL	
362	692467	4739193	267	74	Jn	DFL	
362	692467	4739193	269	38	Jn	DFL	
362	692467	4739193	352	40	Jn	DFL	
363	692424	4739178	52	40	Jgs	DFL	
363	692424	4739178	62	73	Jgs	DFL	
363	692424	4739178	67	50	Jgs	DFL	
363	692424	4739178	68	60	Jgs	DFL	
363	692424	4739178	258	65	Jgs	DFL	
363	692424	4739178	280	68	Jgs	DFL	
364	692344	4739121	55	48	Js	DFL	
364	692344	4739121	61	72	Js	DFL	
364	692344	4739121	62	76	Js	DFL	
364	692344	4739121	65	80	Js	DFL	
364	692344	4739121	66	74	Js	DFL	
364	692344	4739121	66	80	Js	DFL	
364	692344	4739121	73	60	Js	DFL	
364	692344	4739121	74	80	Js	DFL	
364	692344	4739121	234	59	Js	DFL	
364	692344	4739121	243	43	Js	DFL	
364	692344	4739121	243	68	Js	DFL	
364	692344	4739121	249	72	Js	DFL	
364	692344	4739121	252	72	Js	DFL	
365	692391	4739032	48	75	Js	DFL	
365	692391	4739032	58	71	Js	DFL	
365	692391	4739032	64	81	Js	DFL	

Stn	Easting	Northing	Strike	Dip Angle	Formation	Area	Faulted
365	692391	4739032	64	86	Js	DFL	
365	692391	4739032	65	50	Js	DFL	
365	692391	4739032	67	86	Js	DFL	
365	692391	4739032	74	75	Js	DFL	
365	692391	4739032	250	68	Js	DFL	
366	692399	4739021	53	74	Js	DFL	
366	692399	4739021	54	90	Js	DFL	
366	692399	4739021	55	80	Js	DFL	
366	692399	4739021	58	86	Js	DFL	
366	692399	4739021	59	70	Js	DFL	
366	692399	4739021	62	84	Js	DFL	
366	692399	4739021	64	82	Js	DFL	
366	692399	4739021	66	42	Js	DFL	
366	692399	4739021	67	83	Js	DFL	
366	692399	4739021	75	39	Js	DFL	
366	692399	4739021	234	90	Js	DFL	
366	692399	4739021	250	82	Js	DFL	
366	692399	4739021	251	82	Js	DFL	
367	694051	4737609	65	90	Jn	DBL	
367	694051	4737609	70	67	Jn	DBL	
367	694051	4737609	76	67	Jn	DBL	
367	694051	4737609	92	66	Jn	DBL	
367	694051	4737609	109	77	Jn	DBL	
367	694051	4737609	117	72	Jn	DBL	
367	694051	4737609	127	66	Jn	DBL	
367	694051	4737609	237	86	Jn	DBL	
367	694051	4737609	238	80	Jn	DBL	
367	694051	4737609	243	84	Jn	DBL	
367	694051	4737609	245	90	Jn	DBL	

Stn	Easting	Northing	Strike	Dip Angle	Formation	Area	Faulted
367	694051	4737609	247	86	Jn	DBL	
368	694062	4737591	56	86	Jn	DBL	
368	694062	4737591	70	85	Jn	DBL	
368	694062	4737591	129	76	Jn	DBL	
368	694062	4737591	254	87	Jn	DBL	
370	694216	4737309	66	70	Jn	DBL	
370	694216	4737309	84	62	Jn	DBL	
370	694216	4737309	155	84	Jn	DBL	
370	694216	4737309	249	80	Jn	DBL	
370	694216	4737309	253	78	Jn	DBL	
370	694216	4737309	261	66	Jn	DBL	
370	694216	4737309	266	78	Jn	DBL	
370	694216	4737309	267	84	Jn	DBL	
370	694216	4737309	270	80	Jn	DBL	
370	694216	4737309	294	80	Jn	DBL	
371	694250	4737250	80	90	Jn	DBL	
371	694250	4737250	90	80	Jn	DBL	
371	694250	4737250	260	90	Jn	DBL	
371	694250	4737250	345	28	Jn	DBL	
372	694270	4737203	77	74	Jn	DBL	
372	694270	4737203	80	80	Jn	DBL	
372	694270	4737203	122	49	Jn	DBL	
372	694270	4737203	190	55	Jn	DBL	
372	694270	4737203	220	83	Jn	DBL	
372	694270	4737203	223	77	Jn	DBL	
372	694270	4737203	225	79	Jn	DBL	
373	694328	4737135	57	86	Jn	DBL	
373	694328	4737135	59	76	Jn	DBL	
373	694328	4737135	66	88	Jn	DBL	

Stn	Easting	Northing	Strike	Dip Angle	Formation	Area	Faulted
373	694328	4737135	80	70	Jn	DBL	
373	694328	4737135	86	68	Jn	DBL	
373	694328	4737135	223	60	Jn	DBL	
373	694328	4737135	248	77	Jn	DBL	
373	694328	4737135	340	38	Jn	DBL	
374	694403	4737050	80	80	Jn	DBL	
374	694403	4737050	85	78	Jn	DBL	
374	694403	4737050	85	79	Jn	DBL	
375	694450	4736967	69	85	Jn	DBL	
375	694450	4736967	72	82	Jn	DBL	
375	694450	4736967	92	66	Jn	DBL	
375	694450	4736967	230	86	Jn	DBL	
375	694450	4736967	264	76	Jn	DBL	
376	694500	4736923	168	50	Jn	DBL	
376	694500	4736923	255	89	Jn	DBL	
377	694530	4736895	55	90	Jn	DBL	
377	694530	4736895	235	90	Jn	DBL	
377	694530	4736895	250	80	Jn	DBL	
378	694559	4736869	67	84	Jn	DBL	
378	694559	4736869	107	67	Jn	DBL	
379	694786	4737025	45	80	Jgs	DBL	
379	694786	4737025	160	80	Jgs	DBL	
379	694786	4737025	162	84	Jgs	DBL	
379	694786	4737025	183	81	Jgs	DBL	
380	694778	4737050	22	82	Jgs	DBL	
380	694778	4737050	40	75	Jgs	DBL	
382	694622	4737207	316	74	Js	DBL	
383	694586	4737298	210	84	Js	DBL	
385	694457	4737348	74	68	Jgs	DBL	

Stn	Easting	Northing	Strike	Dip Angle	Formation	Area	Faulted
385	694457	4737348	75	86	Jgs	DBL	
385	694457	4737348	222	87	Jgs	DBL	
385	694457	4737348	223	80	Jgs	DBL	
387	694364	4737519	72	86	Js	DBL	
387	694364	4737519	88	78	Js	DBL	
387	694364	4737519	175	46	Js	DBL	
388	694327	4737556	74	80	Jgs	DBL	
388	694327	4737556	77	64	Jgs	DBL	
388	694327	4737556	90	62	Jgs	DBL	
388	694327	4737556	190	54	Jgs	DBL	
388	694327	4737556	197	72	Jgs	DBL	
388	694327	4737556	228	85	Jgs	DBL	
388	694327	4737556	235	70	Jgs	DBL	
389	694258	4737685	56	80	Jgs	DBL	
389	694258	4737685	65	84	Jgs	DBL	
389	694258	4737685	184	60	Jgs	DBL	
393	693008	4738247	70	78	Js	DFL	y
393	693008	4738247	258	62	Js	DFL	y
394	692945	4738156	30	60	Js	DFL	y
394	692945	4738156	34	70	Js	DFL	y
394	692945	4738156	40	82	Js	DFL	y
394	692945	4738156	42	90	Js	DFL	y
394	692945	4738156	221	74	Js	DFL	y
394	692945	4738156	222	90	Js	DFL	y
394	692945	4738156	246	80	Js	DFL	y
394	692945	4738156	261	78	Js	DFL	y
394	692945	4738156	267	54	Js	DFL	y
395	693001	4738036	32	60	Js	DFL	y
395	693001	4738036	56	83	Js	DFL	y

Stn	Easting	Northing	Strike	Dip Angle	Formation	Area	Faulted
395	693001	4738036	62	70	Js	DFL	y
395	693001	4738036	65	83	Js	DFL	y
395	693001	4738036	69	88	Js	DFL	y
395	693001	4738036	268	36	Js	DFL	y
397	693171	4738334	50	89	Jn	DFL	
397	693171	4738334	65	82	Jn	DFL	
397	693171	4738334	232	80	Jn	DFL	
397	693171	4738334	242	62	Jn	DFL	
397	693171	4738334	250	68	Jn	DFL	
397	693171	4738334	270	64	Jn	DFL	
399	693562	4736232	70	22	Kms	DFL	
399	693562	4736232	335	14	Kms	DFL	
401	693524	4736373	48	60	Kms	DFL	
401	693524	4736373	65	56	Kms	DFL	
401	693524	4736373	265	70	Kms	DFL	
401	693524	4736373	324	22	Kms	DFL	
401	693524	4736373	356	10	Kms	DFL	
404	693327	4736900	336	50	Kms	DFL	
405	693310	4736937	245	80	Kms	DFL	
405	693310	4736937	271	70	Kms	DFL	
405	693310	4736937	273	56	Kms	DFL	
405	693310	4736937	297	64	Kms	DFL	
405	693310	4736937	340	40	Kms	DFL	
405	693310	4736937	346	36	Kms	DFL	
405	693310	4736937	347	54	Kms	DFL	
405	693310	4736937	350	36	Kms	DFL	
407	693186	4737284	56	78	Kms	DFL	
407	693186	4737284	295	56	Kms	DFL	
407	693186	4737284	347	56	Kms	DFL	

Stn	Easting	Northing	Strike	Dip Angle	Formation	Area	Faulted
408	693148	4737380	285	63	Kms	DFL	
408	693148	4737380	286	84	Kms	DFL	
408	693148	4737380	290	75	Kms	DFL	
408	693148	4737380	355	52	Kms	DFL	
408	693148	4737380	359	45	Kms	DFL	
410	692956	4737730	55	80	Kms	DFL	
410	692956	4737730	58	76	Kms	DFL	
410	692956	4737730	250	74	Kms	DFL	
410	692956	4737730	251	75	Kms	DFL	
410	692956	4737730	264	86	Kms	DFL	
410	692956	4737730	326	52	Kms	DFL	
410	692956	4737730	336	60	Kms	DFL	
410	692956	4737730	344	50	Kms	DFL	
412	692944	4737471	66	54	Km	DFL	
412	692944	4737471	255	55	Km	DFL	
413	692989	4737396	247	61	Km	DFL	
413	692989	4737396	258	62	Km	DFL	
413	692989	4737396	259	58	Km	DFL	
413	692989	4737396	260	60	Km	DFL	
414	693025	4737312	256	70	Km	DFL	
414	693025	4737312	264	76	Km	DFL	
414	693025	4737312	314	38	Km	DFL	
415	693065	4737235	250	74	Km	DFL	
415	693065	4737235	252	68	Km	DFL	
416	693208	4736873	250	75	Km	DFL	
416	693208	4736873	254	76	Km	DFL	
418	693315	4736621	258	77	Km	DFL	
418	693315	4736621	259	73	Km	DFL	
418	693315	4736621	260	70	Km	DFL	

Stn	Easting	Northing	Strike	Dip Angle	Formation	Area	Faulted
419	693401	4736342	232	52	Km	DFL	
419	693401	4736342	235	47	Km	DFL	
420	693449	4736260	237	65	Km	DFL	
420	693449	4736260	240	66	Km	DFL	
425	694147	4734630	185	89	Kms	DFL	
427	694207	4734559	34	48	Kms	DFL	
435	691055	4742567	327	72	Kms	DFL	
435	691055	4742567	330	68	Kms	DFL	
435	691055	4742567	333	67	Kms	DFL	
435	691055	4742567	334	72	Kms	DFL	
436	691056	4742678	331	56	Kms	DFL	
436	691056	4742678	334	53	Kms	DFL	
436	691056	4742678	336	57	Kms	DFL	
437	691074	4742731	328	62	Kms	DFL	
437	691074	4742731	331	65	Kms	DFL	
437	691074	4742731	331	68	Kms	DFL	
438	691099	4742800	14	58	Kms	DFL	
438	691099	4742800	327	64	Kms	DFL	
438	691099	4742800	330	61	Kms	DFL	
441	691240	4743060	13	75	Kms	DFL	
441	691240	4743060	15	78	Kms	DFL	
442	691216	4743146	10	84	Kms	DFL	
442	691216	4743146	12	80	Kms	DFL	
442	691216	4743146	15	85	Kms	DFL	
446	691359	4742955	347	85	Kt	DFL	
446	691359	4742955	349	84	Kt	DFL	
446	691359	4742955	352	84	Kt	DFL	
447	691335	4742929	346	75	Kt	DFL	
447	691335	4742929	350	84	Kt	DFL	

Stn	Easting	Northing	Strike	Dip Angle	Formation	Area	Faulted
450	691171	4742707	7	53	Kt	DFL	
450	691171	4742707	8	50	Kt	DFL	
450	691171	4742707	10	54	Kt	DFL	
466	692746	4740498	161	54	Kms	DBL	
466	692746	4740498	166	57	Kms	DBL	
489	693935	4738340	63	76	Js	DBL	
489	693935	4738340	73	76	Js	DBL	
489	693935	4738340	215	67	Js	DBL	
492	693803	4738422	66	77	Jgs	DBL	
492	693803	4738422	221	77	Jgs	DBL	
493	693833	4738373	74	80	Jgs	DBL	
493	693833	4738373	103	52	Jgs	DBL	
493	693833	4738373	247	89	Jgs	DBL	
493	693833	4738373	250	89	Jgs	DBL	
495	693921	4738213	55	90	Jgs	DBL	
495	693921	4738213	200	60	Jgs	DBL	
495	693921	4738213	235	90	Jgs	DBL	
495	693921	4738213	240	84	Jgs	DBL	
498	693855	4738166	63	86	Jn	DBL	
498	693855	4738166	67	82	Jn	DBL	
498	693855	4738166	68	87	Jn	DBL	
501	693784	4738629	59	75	Js	DBL	
501	693784	4738629	61	72	Js	DBL	
501	693784	4738629	65	64	Js	DBL	
504	693700	4738802	104	46	Jm	DBL	
519	692306	4740823	83	81	Jm	DBL	
519	692306	4740823	88	74	Jm	DBL	
519	692306	4740823	90	78	Jm	DBL	
521	686965	4736093	235	88	Kf	DPSLP	

Stn	Easting	Northing	Strike	Dip Angle	Formation	Area	Faulted
522	687687	4736712	219	84	Kf	DPSLP	
522	687687	4736712	220	88	Kf	DPSLP	
522	687687	4736712	220	88	Kf	DPSLP	
522	687687	4736712	221	84	Kf	DPSLP	
522	687687	4736712	222	83	Kf	DPSLP	
522	687687	4736712	245	86	Kf	DPSLP	
522	687687	4736712	350	86	Kf	DPSLP	
523	687616	4736485	55	90	Kf	DPSLP	
523	687616	4736485	220	70	Kf	DPSLP	
523	687616	4736485	222	82	Kf	DPSLP	
523	687616	4736485	223	80	Kf	DPSLP	
523	687616	4736485	224	77	Kf	DPSLP	
523	687616	4736485	225	80	Kf	DPSLP	
523	687616	4736485	230	86	Kf	DPSLP	
523	687616	4736485	235	90	Kf	DPSLP	
524	687651	4736436	50	90	Kf	DPSLP	
524	687651	4736436	110	74	Kf	DPSLP	
524	687651	4736436	220	87	Kf	DPSLP	
524	687651	4736436	223	88	Kf	DPSLP	
524	687651	4736436	224	87	Kf	DPSLP	
524	687651	4736436	225	87	Kf	DPSLP	
524	687651	4736436	225	88	Kf	DPSLP	
524	687651	4736436	226	80	Kf	DPSLP	
524	687651	4736436	230	88	Kf	DPSLP	
524	687651	4736436	230	90	Kf	DPSLP	
525	687626	4736454	223	84	Kf	DPSLP	
525	687626	4736454	224	87	Kf	DPSLP	
525	687626	4736454	225	87	Kf	DPSLP	
525	687626	4736454	225	89	Kf	DPSLP	

Stn	Easting	Northing	Strike	Dip Angle	Formation	Area	Faulted
525	687626	4736454	226	88	Kf	DPSLP	
525	687626	4736454	228	88	Kf	DPSLP	
525	687626	4736454	230	84	Kf	DPSLP	
525	687626	4736454	233	82	Kf	DPSLP	
525	687626	4736454	236	85	Kf	DPSLP	
525	687626	4736454	245	84	Kf	DPSLP	
526	687384	4739342	110	76	Kf	DPSLP	
531	686146	4739711	210	74	Kf	DPSLP	
531	686146	4739711	213	70	Kf	DPSLP	
532	686021	4739745	45	90	Kf	DPSLP	
532	686021	4739745	85	74	Kf	DPSLP	
532	686021	4739745	85	88	Kf	DPSLP	
532	686021	4739745	215	86	Kf	DPSLP	
532	686021	4739745	217	72	Kf	DPSLP	
532	686021	4739745	220	88	Kf	DPSLP	
532	686021	4739745	225	90	Kf	DPSLP	
532	686021	4739745	226	86	Kf	DPSLP	
532	686021	4739745	325	12	Kf	DPSLP	
533	686457	4740852	155	74	Kf	DPSLP	
535	685927	4739792	83	80	Kf	DPSLP	
536	685900	4739766	187	88	Kf	DPSLP	
537	685895	4739839	190	76	Kf	DPSLP	
539	685670	4739828	77	82	Kf	DPSLP	
539	685670	4739828	80	82	Kf	DPSLP	
539	685670	4739828	207	84	Kf	DPSLP	
540	685644	4739880	77	88	Kf	DPSLP	
540	685644	4739880	197	80	Kf	DPSLP	
542	685687	4740085	220	86	Kf	DPSLP	
542	685687	4740085	240	86	Kf	DPSLP	

Stn	Easting	Northing	Strike	Dip Angle	Formation	Area	Faulted
545	686502	4739198	105	78	Kf	DPSLP	
547	686607	4738445	75	84	Kf	DPSLP	
547	686607	4738445	85	80	Kf	DPSLP	
548	686558	4738535	90	88	Kf	DPSLP	
548	686558	4738535	264	88	Kf	DPSLP	
549	694341	4736825	50	88	Ta	DBL	
549	694341	4736825	53	88	Ta	DBL	
549	694341	4736825	116	57	Ta	DBL	
549	694341	4736825	130	67	Ta	DBL	
549	694341	4736825	210	74	Ta	DBL	
551	692696	4737612	65	80	Kf	DFL	
551	692696	4737612	154	70	Kf	DFL	
551	692696	4737612	289	88	Kf	DFL	
552	692790	4737452	64	90	Kf	DFL	
552	692790	4737452	232	40	Kf	DFL	
552	692790	4737452	244	90	Kf	DFL	
552	692790	4737452	245	50	Kf	DFL	
555	692925	4737183	260	45	Kf	DFL	
556	692997	4737060	235	79	Kf	DFL	
556	692997	4737060	242	89	Kf	DFL	
556	692997	4737060	245	74	Kf	DFL	
557	693035	4736973	65	52	Kf	DFL	
557	693035	4736973	238	76	Kf	DFL	
557	693035	4736973	244	74	Kf	DFL	
557	693035	4736973	260	74	Kf	DFL	
558	693118	4736846	246	72	Kf	DFL	
558	693118	4736846	253	70	Kf	DFL	
558	693118	4736846	260	50	Kf	DFL	
559	693168	4736717	255	64	Kf	DFL	

Stn	Easting	Northing	Strike	Dip Angle	Formation	Area	Faulted
567	693850	4737445	95	77	Trp	DBL	
567	693850	4737445	337	84	Trp	DBL	
568	693933	4737446	65	89	Trp	DBL	
568	693933	4737446	85	72	Trp	DBL	
568	693933	4737446	95	70	Trp	DBL	
568	693933	4737446	100	66	Trp	DBL	
568	693933	4737446	254	89	Trp	DBL	
569	693954	4737424	110	76	Trp	DBL	
569	693954	4737424	230	72	Trp	DBL	
569	693954	4737424	240	74	Trp	DBL	
570	693981	4737426	110	80	Trp	DBL	
570	693981	4737426	115	78	Trp	DBL	
570	693981	4737426	238	80	Trp	DBL	
570	693981	4737426	240	67	Trp	DBL	
570	693981	4737426	255	80	Trp	DBL	
570	693981	4737426	285	82	Trp	DBL	
571	694012	4737369	55	89	Trp	DBL	
571	694012	4737369	60	88	Trp	DBL	
571	694012	4737369	130	70	Trp	DBL	
571	694012	4737369	240	84	Trp	DBL	
571	694012	4737369	242	82	Trp	DBL	
572	694039	4737306	47	48	Trp	DBL	
572	694039	4737306	64	74	Trp	DBL	
572	694039	4737306	75	86	Trp	DBL	
572	694039	4737306	93	80	Trp	DBL	
572	694039	4737306	210	84	Trp	DBL	
572	694039	4737306	245	80	Trp	DBL	
573	694120	4737195	87	78	Ta	DBL	YES
573	694120	4737195	257	76	Ta	DBL	YES

Stn	Easting	Northing	Strike	Dip Angle	Formation	Area	Faulted
573	694120	4737195	272	89	Ta	DBL	YES
574	694157	4737144	315	22	Fault	DBL	YES
575	694142	4737117	330	22	Fault	DBL	YES
576	693870	4737181	255	78	Ta	DFL	
577	693874	4737165	60	76	Ta	DFL	
577	693874	4737165	70	70	Ta	DFL	
577	693874	4737165	75	89	Ta	DFL	
577	693874	4737165	255	89	Ta	DFL	
577	693874	4737165	260	84	Ta	DFL	
577	693874	4737165	265	86	Ta	DFL	
578	693885	4737130	254	88	Ta	DFL	
579	693979	4736778	260	78	Ta	DFL	
579	693979	4736778	272	70	Ta	DFL	
579	693979	4736778	322	22	Ta	DFL	
581	690749	4747520	180	72	Kf	HBL	
582	690743	4747415	172	74	Kf	HBL	
583	690750	4747334	270	80	Kf	HBL	
584	690765	4747207	160	64	Kf	HBL	
585	690782	4747046	100	80	Kf	HBL	
586	690808	4746897	165	70	Kf	HBL	
587	690806	4746719	65	80	Kf	HBL	
587	690806	4746719	242	82	Kf	HBL	
592	690592	4746389	95	66	Kf	HBL	
592	690592	4746389	95	76	Kf	HBL	
592	690592	4746389	103	72	Kf	HBL	
594	690364	4747070	104	70	Kf	HBL	
594	690364	4747070	200	66	Kf	HBL	
594	690364	4747070	251	82	Kf	HBL	
594	690364	4747070	257	86	Kf	HBL	

Stn	Easting	Northing	Strike	Dip Angle	Formation	Area	Faulted
594	690364	4747070	260	86	Kf	HBL	
599	689017	4747596	95	76	Jn	HBL	
599	689017	4747596	110	76	Jn	HBL	
600	689103	4747722	84	89	Jn	HBL	
600	689103	4747722	90	84	Jn	HBL	
600	689103	4747722	275	89	Jn	HBL	
602	689102	4747595	80	76	Jn	HBL	
602	689102	4747595	84	70	Jn	HBL	
602	689102	4747595	85	76	Jn	HBL	
602	689102	4747595	254	74	Jn	HBL	
605	689385	4747632	86	76	Js	HBL	
605	689385	4747632	90	76	Js	HBL	
605	689385	4747632	90	84	Js	HBL	
605	689385	4747632	94	78	Js	HBL	
606	689375	4747558	110	78	Js	HBL	
606	689375	4747558	267	88	Js	HBL	
608	689430	4747299	65	83	Js	HBL	
608	689430	4747299	67	84	Js	HBL	
608	689430	4747299	76	80	Js	HBL	
608	689430	4747299	90	82	Js	HBL	
608	689430	4747299	277	83	Js	HBL	
608	689430	4747299	278	80	Js	HBL	
608	689430	4747299	278	86	Js	HBL	
610	689569	4747788	80	76	Kt	HBL	
610	689569	4747788	85	77	Kt	HBL	
610	689569	4747788	172	56	Kt	HBL	
611	689464	4748093	105	76	Kt	HBL	
611	689464	4748093	120	84	Kt	HBL	
611	689464	4748093	209	70	Kt	HBL	

Stn	Easting	Northing	Strike	Dip Angle	Formation	Area	Faulted
612	689425	4748194	82	85	Kt	HBL	
612	689425	4748194	83	89	Kt	HBL	
612	689425	4748194	180	78	Kt	HBL	
613	689397	4748298	95	86	Kt	HBL	
613	689397	4748298	95	87	Kt	HBL	
613	689397	4748298	180	67	Kt	HBL	
614	689399	4748408	75	80	Kt	HBL	
614	689399	4748408	84	78	Kt	HBL	
614	689399	4748408	90	84	Kt	HBL	
614	689399	4748408	206	76	Kt	HBL	
615	689361	4748508	50	90	Kt	HBL	
615	689361	4748508	60	89	Kt	HBL	
615	689361	4748508	66	86	Kt	HBL	
615	689361	4748508	67	80	Kt	HBL	
615	689361	4748508	230	90	Kt	HBL	
616	689365	4748618	102	90	Kt	HBL	
616	689365	4748618	108	87	Kt	HBL	
616	689365	4748618	188	68	Kt	HBL	
616	689365	4748618	227	80	Kt	HBL	
616	689365	4748618	282	90	Kt	HBL	
617	689330	4748732	67	84	Kt	HBL	
617	689330	4748732	70	90	Kt	HBL	
617	689330	4748732	80	80	Kt	HBL	
617	689330	4748732	80	89	Kt	HBL	
617	689330	4748732	85	82	Kt	HBL	
617	689330	4748732	100	82	Kt	HBL	
617	689330	4748732	106	84	Kt	HBL	
617	689330	4748732	245	89	Kt	HBL	
617	689330	4748732	250	90	Kt	HBL	

Stn	Easting	Northing	Strike	Dip Angle	Formation	Area	Faulted
618	695544	4736660	55	84	Jm	DBL	
618	695544	4736660	65	84	Jm	DBL	
618	695544	4736660	255	87	Jm	DBL	
618	695544	4736660	270	80	Jm	DBL	
619	695540	4736586	135	80	Js	DBL	
619	695540	4736586	235	88	Js	DBL	
620	695487	4736641	60	88	Js	DBL	
620	695487	4736641	70	87	Js	DBL	
620	695487	4736641	72	80	Js	DBL	
620	695487	4736641	210	74	Js	DBL	
620	695487	4736641	241	89	Js	DBL	
621	695489	4736401	60	75	Js	DBL	
621	695489	4736401	64	80	Js	DBL	
621	695489	4736401	67	82	Js	DBL	
621	695489	4736401	73	86	Js	DBL	
621	695489	4736401	165	60	Js	DBL	
622	695438	4736467	55	88	Js	DBL	
622	695438	4736467	67	89	Js	DBL	
622	695438	4736467	190	73	Js	DBL	
622	695438	4736467	195	74	Js	DBL	
622	695438	4736467	230	84	Js	DBL	
623	695375	4736508	50	89	Js	DBL	
623	695375	4736508	60	81	Js	DBL	
623	695375	4736508	144	60	Js	DBL	
623	695375	4736508	155	74	Js	DBL	
623	695375	4736508	190	74	Js	DBL	
624	695320	4736579	75	69	Jgs	DBL	
624	695320	4736579	145	73	Jgs	DBL	
624	695320	4736579	164	75	Jgs	DBL	

Stn	Easting	Northing	Strike	Dip Angle	Formation	Area	Faulted
625	695239	4736638	40	89	Jgs	DBL	
625	695239	4736638	83	82	Jgs	DBL	
625	695239	4736638	94	78	Jgs	DBL	
625	695239	4736638	100	80	Jgs	DBL	
625	695239	4736638	110	76	Jgs	DBL	
625	695239	4736638	165	66	Jgs	DBL	
625	695239	4736638	205	74	Jgs	DBL	
625	695239	4736638	222	82	Jgs	DBL	
625	695239	4736638	224	85	Jgs	DBL	
625	695239	4736638	247	81	Jgs	DBL	
626	695130	4736803	15	88	Jgs	DBL	
626	695130	4736803	50	84	Jgs	DBL	
626	695130	4736803	55	84	Jgs	DBL	
626	695130	4736803	57	80	Jgs	DBL	
626	695130	4736803	60	74	Jgs	DBL	
626	695130	4736803	104	64	Jgs	DBL	
626	695130	4736803	153	60	Jgs	DBL	
626	695130	4736803	203	80	Jgs	DBL	
627	695491	4736783	244	85	Jm	DBL	
628	695771	4736999	70	86	Kms	DBL	
629	695671	4737123	75	84	Kms	DBL	
629	695671	4737123	90	82	Kms	DBL	
629	695671	4737123	105	80	Kms	DBL	
629	695671	4737123	160	70	Kms	DBL	
629	695671	4737123	210	88	Kms	DBL	
629	695671	4737123	280	84	Kms	DBL	
630	695591	4737197	165	70	Kms	DBL	
630	695591	4737197	204	83	Kms	DBL	
630	695591	4737197	230	80	Kms	DBL	

Stn	Easting	Northing	Strike	Dip Angle	Formation	Area	Faulted
632	695459	4737333	13	84	Kms	DBL	
632	695459	4737333	95	78	Kms	DBL	
633	695426	4737857	145	68	Kms	DBL	
633	695426	4737857	230	86	Kms	DBL	
635	695103	4737935	120	86	Kms	DBL	
635	695103	4737935	207	85	Kms	DBL	
636	694882	4738014	74	84	Kms	DBL	
636	694882	4738014	160	72	Kms	DBL	
637	694840	4738071	74	84	Kms	DBL	
637	694840	4738071	160	72	Kms	DBL	
638	694441	4738233	210	68	Kms	DBL	
642	694401	4736694	22	70	Ta	DBL	
642	694401	4736694	64	89	Ta	DBL	
642	694401	4736694	117	70	Ta	DBL	
642	694401	4736694	125	60	Ta	DBL	
642	694401	4736694	225	85	Ta	DBL	
642	694401	4736694	245	90	Ta	DBL	
642	694401	4736694	340	70	Ta	DBL	
643	694415	4736657	60	88	Ta	DBL	
643	694415	4736657	115	70	Ta	DBL	
644	694368	4736430	125	80	Trp	DBL	
644	694368	4736430	130	87	Trp	DBL	
644	694368	4736430	238	88	Trp	DBL	
645	694378	4736298	80	60	Trp	DBL	
645	694378	4736298	105	80	Trp	DBL	
645	694378	4736298	195	64	Trp	DBL	
646	694367	4736275	114	90	Trp	DBL	
646	694367	4736275	117	88	Trp	DBL	
646	694367	4736275	200	78	Trp	DBL	

Stn	Easting	Northing	Strike	Dip Angle	Formation	Area	Faulted
646	694367	4736275	304	86	Trp	DBL	
647	694357	4736227	84	70	Ta	DFL	
647	694357	4736227	255	80	Ta	DFL	
647	694357	4736227	258	82	Ta	DFL	
647	694357	4736227	260	84	Ta	DFL	
647	694357	4736227	260	88	Ta	DFL	
647	694357	4736227	340	80	Ta	DFL	
650	694073	4736396	187	84	Ta	DFL	
650	694073	4736396	277	64	Ta	DFL	
650	694073	4736396	281	66	Ta	DFL	
651	692144	4738956	73	76	Kms	DFL	
651	692144	4738956	268	66	Kms	DFL	
652	692357	4738598	55	84	Kms	DFL	
652	692357	4738598	238	80	Kms	DFL	
653	691973	4739310	40	86	Kms	DFL	
653	691973	4739310	67	84	Kms	DFL	
654	691900	4739432	70	85	Kms	DFL	
654	691900	4739432	75	82	Kms	DFL	
655	691716	4739727	24	60	Kms	DFL	
655	691716	4739727	25	74	Kms	DFL	
655	691716	4739727	47	70	Kms	DFL	
655	691716	4739727	90	89	Kms	DFL	
656	691668	4739343	63	40	Kf	DFL	
656	691668	4739343	72	74	Kf	DFL	

Appendix C

Contoured equal area stereographic projections poles to fracture planes collected for each domain and used in the fracture analysis. Fracture data was not rotated to remove tectonic tilting in these diagrams because of lack of control on bedding orientation during formation. The domains are labeled for each figure below: 1) Wind River dip slope, 2) Dallas Dome forelimb, and 3) Dallas Dome backlimb. Data concentrations were determined using the Gaussian K=100 method where the fractional area is 1% of the hemisphere and “n” is the number of data points for each count. Densities are counted by multiples of sigma “S” over “E”, which is the expected count. Scales to the right of each diagram represent the densities of these multiples of sigma over the expected value.

1: Wind River Dip Slope

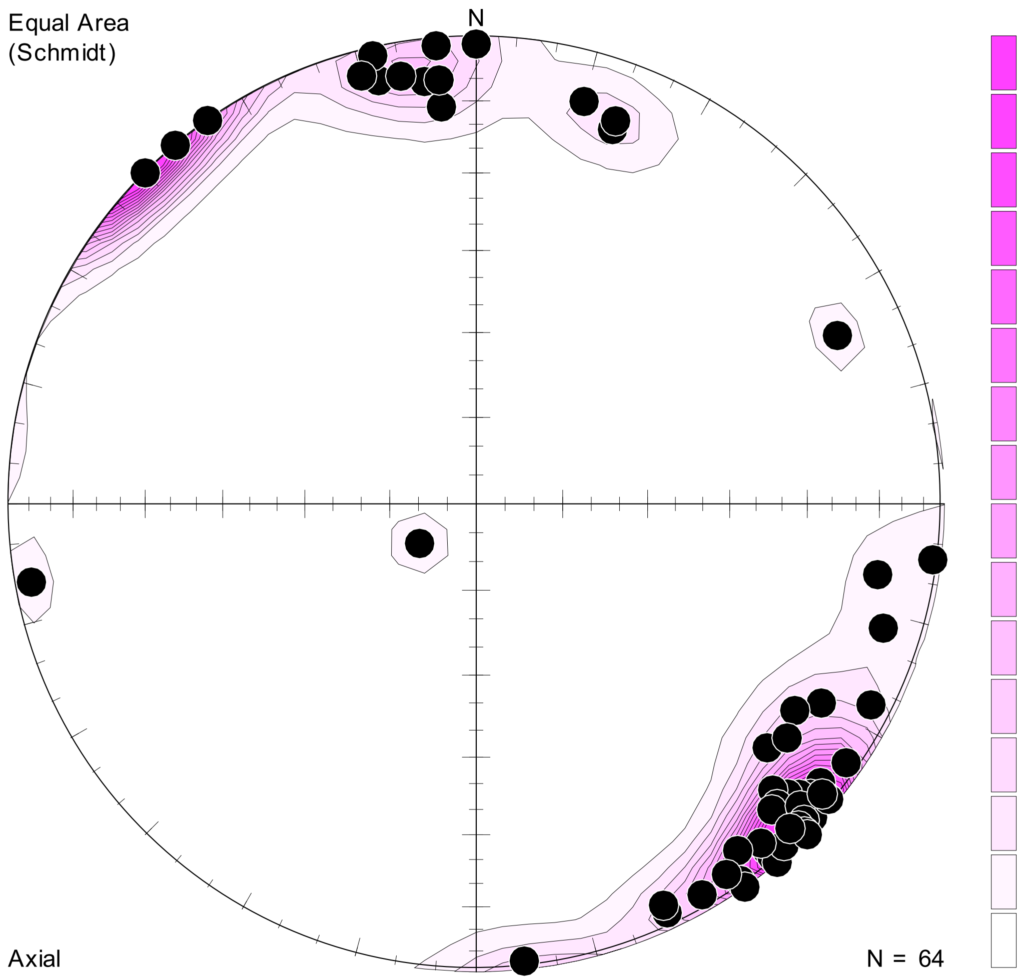

2: Dallas Dome Forelimb

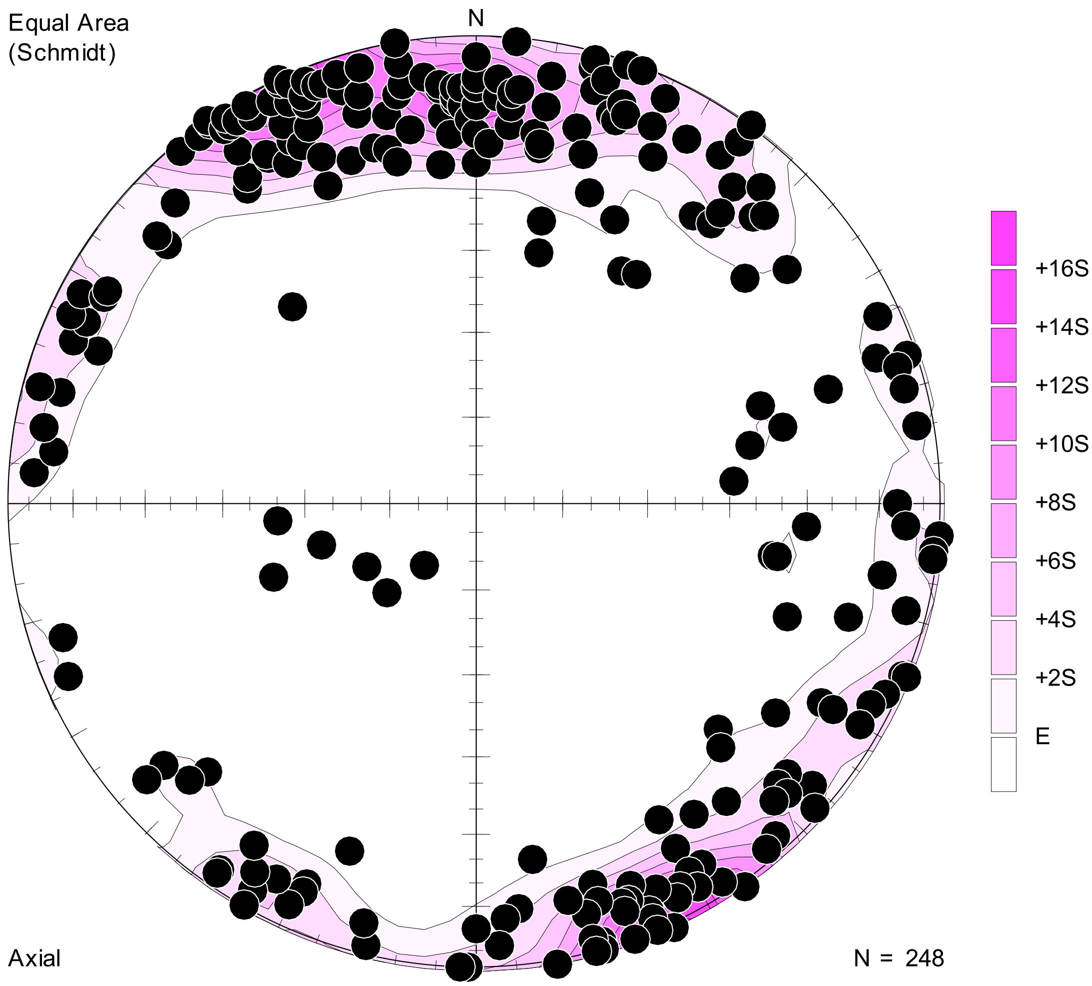

3: Dallas Dome Backlimb

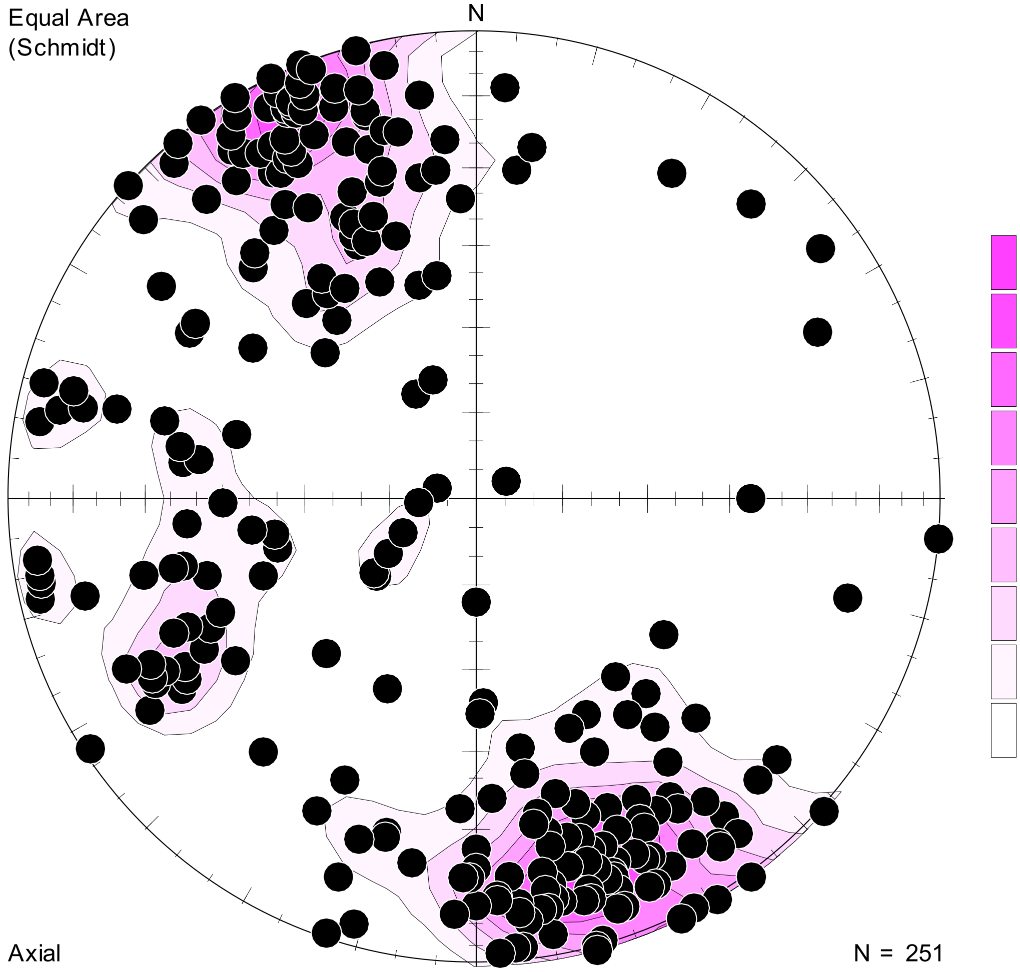

REFERENCE CITED

Abercrombie, S., 1989, Structural analysis of the Sheep Mountain-Beaver Creek thrust area, Fremont County, Wyoming [Master's thesis]: Baylor University : Waco, TX,
United States, 71 p.

Ahlstrand, D. C., 1978, Permian carbonate facies, Wind River basin, Wyoming: Guidebook - Wyoming Geological Association, no. 30, p. 89-99.

Allmendinger, R. W., 1992, Fold and thrust tectonics of the Western United States exclusive of the accreted terranes: GSA, v. G-3, p. 583.

-, 1998, Inverse and forward numerical modeling of trishear fault-propagation folds: Tectonics, v. 17, no. 4, p. 640.

-, 1999a, Numerical analyses of trishear fault-propagation folds; implications for geometry, growth strata, strain evolution, and fracturing: Annual Meeting Expanded Abstracts - American Association of Petroleum Geologists, v. 1999, p. A4.

-, 1999b, Propagation-to-slip ratio and fold style in fault-propagation folds; perspectives gleaned from trishear modeling: Abstracts with Programs - Geological Society of America, v. 31, no. 7, p. 237.

Angelier, J., 1994, Fault slip analysis and palaeostress reconstruction, *in* Hancock, P. L., ed., Pergamon Press : Tarrytown, NY, p. 53.

Antweiler, J. C., Love, J. D., Mosier, E. L., and Campbell, W. L., 1980, Oligocene goldbearing conglomerate, southeast margin of Wind River Mountains, Wyoming: Guidebook - Wyoming Geological Association, no. 31, p. 223-237.

Bell, L. H., and Middleton, L. T., 1978, An introduction to the Cambrian Flathead Sandstone, Wind River basin, Wyoming: Guidebook - Wyoming Geological Association, no. 30, p. 79-88.

Berg, R. R., 1961, Laramide tectonics of the Wind River Mountains, p. 70-80.

-, 1962, Mountain flank thrusting in Rocky Mountain foreland, Wyoming and Colorado: Bulletin of the American Association of Petroleum Geologists, v. 46, no. 11, p. 2019.

Bergbauer, S., and Pollard, D. D., 2004, A new conceptual fold-fracture model including prefolding joints, based on the Emigrant Gap Anticline, Wyoming: Geological Society of America Bulletin, v. 116, no. 3-4, p. 294.

Bird, P., 1983, Horizontal Farallon Plate subduction and Laramide epeirogeny: Abstracts with Programs - Geological Society of America, v. 15, no. 5, p. 404.

-, 1998, Kinematic history of the Laramide Orogeny in latitudes 35 degrees -49 degrees N, Western United States: Tectonics, v. 17, no. 5, p. 780.

Blackstone, D. L., Jr.;, 1993, The Wind River Range, Wyoming; an overview, Guidebook - Wyoming Geological Association: United States, Wyoming Geological Association : Casper, WY, United States, p. 121.

Boyd, D. W., 1993, Paleozoic history of Wyoming: Memoir - Geological Survey of Wyoming, v. 5, p. 164-187.

Brewer, J. A., Smithson, S. B., Oliver, J. E., Kaufman, S., and Brown, L. D., 1980, The Laramide Orogeny; evidence from COCORP deep crustal seismic profiles in the Wind River Mountains, Wyoming: Tectonophysics, v. 62, no. 3-4, p. 165.

Brocka, C.G., 2007, Laramide stress conditions and deformation mechanisms during the formation of Derby and Dallas Domes, Weiser Pass Quadrangle, Wind River Mountains, Wyoming.

Brown, W. G., 1984, Basement involved tectonics, foreland areas: AAPG Continuing Education Course Note Series, v. 26.

-, 1988, Deformational style of Laramide uplifts in the Wyoming foreland: Memoir - Geological Society of America, v. 171, p. 1.

-, 1993, Structural style of Laramide basement-cored uplifts and associated folds: Memoir - Geological Survey of Wyoming, v. 5, p. 312-371.

Bump, A. P., 2003, Reactivation, trishear modeling, and folded basement in Laramide uplifts; implications for the origins of intra-continental faults: GSA Today, v. 13, no. 3, p. 4.

Bunge, H. P., and Grand, S. P., 2000, Mesozoic plate-motion history below the northeast Pacific Ocean from seismic images of the subducted Farallon Slab: Nature, v. 405, no. 6784, p. 337-340.

Cosgrove, J. W., and Ameen, M. S., 2000, A comparison of the geometry, spatial organization and fracture patterns associated with forced folds and buckle folds: Geological Society Special Publications, v. 169, p. 7-21.

Craddock, J. P., and Relle, M., 2003, Fold axis-parallel rotation within the Laramide Derby Dome Fold, Wind River basin, Wyoming, USA: Journal of Structural Geology, v. 25, no. 11, p. 1959.

Cristallini, E. O., and Allmendinger, R. W., 2002, Backlimb trishear; a kinematic model for curved folds developed over angular fault bends: Journal of Structural Geology, v. 24, no. 2, p. 289.

Currie, J. B., Patnode, H. W. and Trump, R. P., 1962, Development of folds in sedimentary strata: Geological Society of America Bulletin, v. 73, p. 655-674.

Curry, W. H., III;, 1990, Early Cretaceous Muddy Sandstone of western Wind River basin, Wyoming: Guidebook - Wyoming Geological Association, v. 41, p. 182.

DeCelles, P. G., 2004, Late Jurassic to Eocene evolution of the Cordilleran thrust belt and foreland basin system, western U.S.A.: American Journal of Science, v. 304, no. 2, p. 105.

Dickinson, W. R., and Snyder, W. S., 1978, Plate tectonics of the Laramide Orogeny: Memoir - Geological Society of America, no. 151, p. 355.

Dunne, W. M., and Hancock, P. L., 1994, Palaeostress analysis of small-scale brittle structures, *in* Hancock, P. L., ed., Pergamon Press : Tarrytown, NY, p. 101.

Erslev, E. A., 1991, Trishear fault-propagation folding: Geology Boulder, v. 19, no. 6, p. 617.

Erslev, E. A., and Rogers, J. L., 1993, Basement-cover geometry of Laramide fault propagation folds: Special Paper - Geological Society of America, v. 280, p. 125.

Hamilton, W., 1981, Plate-tectonic mechanism of Laramide deformation: Contributions to Geology, v. 19, no. 2, p. 87.

Haun, J. D., and Barlow, J. A., Jr.;, 1962, Lower Cretaceous stratigraphy of Wyoming, p. 15-22.

Keefer, W. R., 1970, Structural geology of the Wing River basin, Wyoming: U. S. Geological Survey Professional Paper.

Kightlinger, C. L., 1997, Detailed structural analysis of the Lander-Hudson oil field (and adjacent anticlines); east flank Wind River Mountains, Fremont County, Wyoming.

Love, J. D., and Christiansen, A. C., 1980, Preliminary correlation of stratigraphic units used on 1 and 2 degree geologic quadrangle maps of Wyoming: Wyoming Geological Association Guidebook, Annual Field Conference, v. 31, p. 279-282.

Maxson, J. A., and Tikoff, B., 1996, Hit-and-run collision model for the Laramide Orogeny, Western United States: Geology Boulder, v. 24, no. 11, p. 968.

McElhinny, M. W., and Lock, J., 1995, Four IAGA paleomagnetic databases released in one package: Eos Trans. AGU, v. 76, p. 266.

Meinen, T. W., 1993, Structural analysis of the en echelon arrangement of Dallas and Derby anticlines.

Picard, M. D., 1978, Stratigraphy of Triassic rocks in West-central Wyoming: Guidebook - Wyoming Geological Association, no. 30, p. 101-130.

Ptasynski, H., 1957, Dallas Dome-Derby Dome area, Wyo. Geol. Assoc., Guidebook, 12th Ann. Field Conf., Sept. 1957., WGA, p. 127 - 131.

Ramsay, J. G., 1967, Folding and fracturing of rocks: United States, 568 p.

Roberts, S., 1989, Wyoming geomaps: Geological Survey of Wyoming : Laramie, WY, United States.

Stearns, D. W., 1978, Faulting and forced folding in the Rocky Mountains foreland, in V. Matthews, Ed. Laramide Folding Associated with Basement Block Faulting in the Western United States. Geological Society of America Memoir 15.

Stesky, R. M., 1995, Spheristat 2 User's Manual: Brockville, Ontario, Canada, Pangaea Scientific, 198 p.

Van Alstine, D. R., and de Boer, J., 1978, A new technique for constructing apparent wander paths and the revised Phanerozoic path for North America: Geology, v. 6, p. 137-139.

Willis, J. J., and Groshong, R. H., Jr.;, 1993, Deformational style of the Wind River Uplift and associated flank structures, Wyoming, p. 337.

Winn, R. D., Jr.;, and Smithwick, M. E., 1980, Lower Frontier Formation, southwestern Wyoming; depositional controls on sandstone compositions and on diagenesis: Guidebook - Wyoming Geological Association, no. 31, p. 137-153.